



Mechanistic insights into mitochondrial tRNA^{Ala} 3'-end metabolism deficiency

Received for publication, March 16, 2021, and in revised form, May 10, 2021. Published, Papers in Press, May 21, 2021.
<https://doi.org/10.1016/j.jbc.2021.100816>

Yanchun Ji^{1,2}, Zhipeng Nie², Feilong Meng^{1,2}, Cuifang Hu^{2,3}, Hui Chen², Lihao Jin², Mengquan Chen⁴,
Minglian Zhang⁵, Juanjuan Zhang³, Min Liang³, Meng Wang^{1,2}, and Min-Xin Guan^{1,2,6,7,*}

From the ¹Division of Medical Genetics and Genomics, The Children's Hospital, Zhejiang University School of Medicine and National Clinical Research Center for Child Health, Hangzhou, Zhejiang, China; ²Institute of Genetics, Zhejiang University School of Medicine, Hangzhou, Zhejiang, China; ³School of Ophthalmology and Optometry, Wenzhou Medical University, Wenzhou, Zhejiang, China; ⁴Department of Lab Medicine, Wenzhou Hospital of Traditional Chinese Medicine, Wenzhou, Zhejiang, China; ⁵Department of Ophthalmology, Hebei Provincial Eye Hospital, Xingtai, Hebei, China; ⁶Center for Mitochondrial Genetics, Zhejiang Provincial Key Laboratory of Genetic & Developmental Disorders, Zhejiang University, Hangzhou, Zhejiang, China; ⁷Division of Mitochondrial Biomedicine, Joint Institute of Genetics and Genome Medicine between Zhejiang University and University of Toronto, Hangzhou, Zhejiang, China

Edited by Karin Musier-Forsyth

Mitochondrial tRNA 3'-end metabolism is critical for the formation of functional tRNAs. Deficient mitochondrial tRNA 3'-end metabolism is linked to an array of human diseases, including optic neuropathy, but their pathophysiology remains poorly understood. In this report, we investigated the molecular mechanism underlying the Leber's hereditary optic neuropathy (LHON)-associated tRNA^{Ala} 5587A>G mutation, which changes a highly conserved adenosine at position 73 (A73) to guanine (G73) on the 3'-end of the tRNA acceptor stem. The m.5587A>G mutation was identified in three Han Chinese families with suggested maternal inheritance of LHON. We hypothesized that the m.5587A>G mutation altered tRNA^{Ala} 3'-end metabolism and mitochondrial function. *In vitro* processing experiments showed that the m.5587A>G mutation impaired the 3'-end processing of tRNA^{Ala} precursors by RNase Z and inhibited the addition of CCA by tRNA nucleotidyltransferase (TRNT1). Northern blot analysis revealed that the m.5587A>G mutation perturbed tRNA^{Ala} aminoacylation, as evidenced by decreased efficiency of aminoacylation and faster electrophoretic mobility of mutated tRNA^{Ala} in these cells. The impact of m.5587A>G mutation on tRNA^{Ala} function was further supported by increased melting temperature, conformational changes, and reduced levels of this tRNA. Failures in tRNA^{Ala} metabolism impaired mitochondrial translation, perturbed assembly and activity of oxidative phosphorylation complexes, diminished ATP production and membrane potential, and increased production of reactive oxygen species. These pleiotropic defects elevated apoptotic cell death and promoted mitophagy in cells carrying the m.5587A>G mutation, thereby contributing to visual impairment. Our findings may provide new insights into the pathophysiology of LHON arising from mitochondrial tRNA 3'-end metabolism deficiency.

The maturations of mitochondrial tRNA including 3' end metabolisms are critical for the formation of functional tRNA for the translation (1, 2). Deficient maturations of mitochondrial RNA transcripts have been linked to an array of human diseases, including deafness, hypertension, and vision impairment (3–8). The maturation of human mitochondrial RNA is the multistep processes involved in transcription, nucleolytic processing, and posttranscriptional modifications (2, 9, 10). Human mitochondrial DNA (mtDNA) encoding two rRNAs and 22 tRNAs and 13 structural subunits of oxidative phosphorylation system (OXPHOS) bidirectionally produce the polycistronic heavy (H) and light (L)-strand polycistronic transcripts, catalyzed by mitochondrial transcription machinery (9–14). After transcription, the polycistronic transcript precursors release two rRNAs, 13 mRNAs, and 22 tRNAs, mediated by RNase P and RNase Z, respectively (15, 16). The CCA triple that forms the 3' terminus of tRNA is synthesized by tRNA nucleotidyltransferase (TRNT1) after 3' end cleavage (17–19). A subset of nucleotides in these tRNAs becomes posttranscriptionally modified by tRNA modifier enzymes (20–24). Amino acid attachment to the CCA in the mature tRNAs is catalyzed by mitochondrial aminoacyl-tRNA synthetase (25–27). The deficiencies in the 5' or 3' end metabolism of mitochondrial tRNA precursors have been linked to several clinical abnormalities (2, 28, 29). The tRNA^{Ile} 4263A>G, tRNA^{Ala} 5655A>G, tRNA^{Ser(UCN)}/tRNA^{Tyr} 7516delA and tRNA^{Gln}/tRNA^{Met} 4401A>G mutations perturbed the 5' end processing efficiencies of corresponding tRNA precursors (7, 8, 30, 31). The tRNA^{Ser(UCN)} 7445T>C, tRNA^{Ile} 4269A>G, tRNA^{Ile} 4295A>G, and tRNA^{His} 12192G>A mutation altered the 3' end processing of corresponding tRNA precursors (32–35). Furthermore, mutations in the TRNT1 perturbed the CCA-addition of tRNAs leading to several clinical presentations including the vision impairment (36–38). However, the molecular mechanisms underlying these tRNA maturation deficiencies remain poorly understood.

* For correspondence: Min-Xin Guan, gminxin88@zju.edu.cn.

Mechanism for mitochondrial tRNA 3'-end deficiency

Most recently, we identified a T to C transition at the position 5587 (5587A>G) at the 3' end of tRNA^{Ala} gene in three genetically unrelated Chinese pedigrees displaying Leber's hereditary optic neuropathy (LHON) from a large cohort of Chinese patients (39). As shown in Figure 1, the m.5587A>G mutation affected a highly conserved adenine at position 73 (A73) at acceptor stem of tRNA^{Ala}. The A73 is the site for the tRNA^{Ala} 3' end precursor processing of L-strand transcripts catalyzed by RNase Z, the CCA addition synthesized by TRNT1 and the discriminator base for its cognate aminoacyl-tRNA synthetase (7, 15, 19, 32, 36, 40–42). Therefore, it is anticipated that the A73 to G73 transition of tRNA^{Ala} caused by m.5587A>G mutation leads to pleiotropic effects on the 3' end processing of transcript precursor, CCA addition, aminoacylation, and stability of tRNA^{Ala}. The aberrant tRNA^{Ala} metabolism may result in the impairment of mitochondrial translation, defects in oxidative phosphorylation, oxidative stress, and subsequent failure of cellular energetic processes. To investigate pathogenic mechanism of m.5587A>G mutation, we generated the cybrids by transferring mitochondria from lymphoblastoid cell lines derived from affected matrilineal relative carrying the m.5587A>G mutation and from a control subject lacking the mutation into mtDNA-less ρ^0 206 cells (43, 44). These cybrid lines were analyzed for the effects of the m.5587A>G mutation on the tRNA^{Ala}

metabolisms including the 3' end processing of tRNA precursors, CCA addition, stability, and aminoacylation of tRNA^{Ala}. These cybrids were further assessed for the effects of m.5587A>G mutation on mitochondrial translation, oxidative phosphorylation system (OXPHOS), mitochondrial membrane potential, production of reactive oxidative species (ROS), apoptosis, and autophagy.

Results

Clinical presentation

Three Han Chinese LHON pedigrees bearing the m.5587A>G mutation were identified among a large cohort of 1793 Chinese probands with LHON (39). As shown in Table S1 and Fig. S1, seven of 21 matrilineal relatives exhibited variable penetrance and expressivity of optic neuropathy. In particular, the severity of visual loss ranged from profound visual loss to normal vision. The age at onset of optic neuropathy of seven affected matrilineal relatives bearing the m.5587A>G mutation ranged from 6 to 41 years, with an average of 26 years. These pedigrees exhibited different penetrance of optic neuropathy, ranging from 14.3% to 42.9%, with an average of 33.3%. There was no evidence that any of other members of these families had any other causes to account for vision loss. These matrilineal relatives showed no

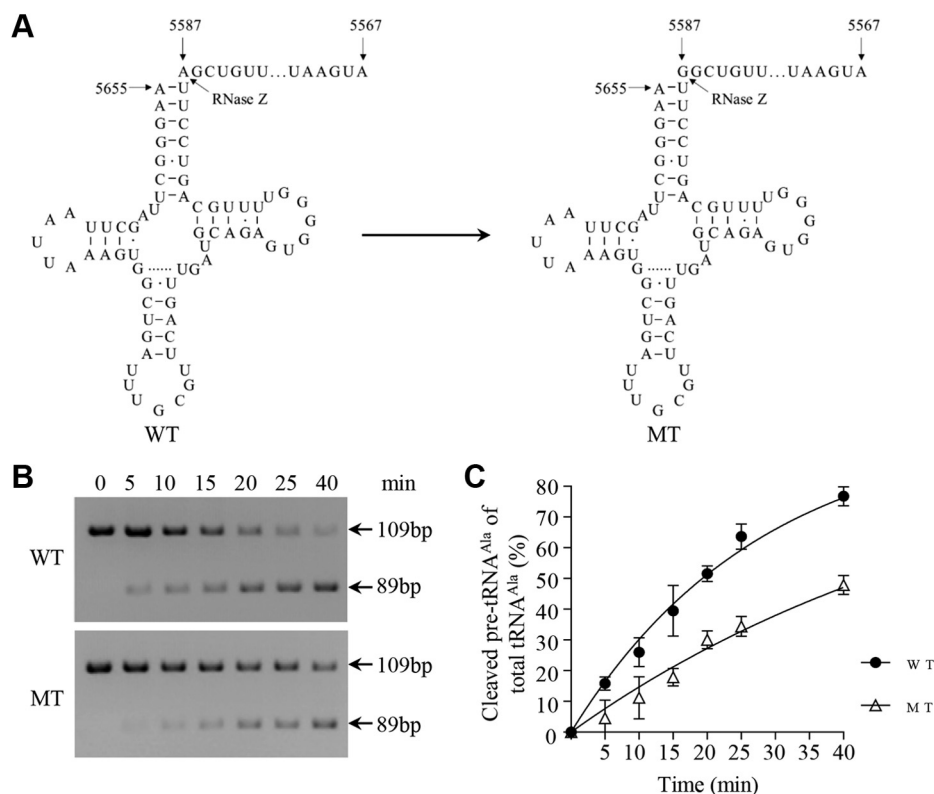


Figure 1. *In vitro* assay for the 3' end processing of mitochondrial tRNA^{Ala} precursors. A, mitochondrial tRNA^{Ala} precursors. Twenty nucleotides (nt) of 3' end trailer of tRNA^{Ala} were shown, including the m.5587A>G substitution. B, *In vitro* 3' end processing assays. Processing assays with mitochondrial RNase Z were undertaken in parallel for wild-type and mutant substrates. Samples were withdrawn and stopped after 5, 10, 15, 20, 25, or 40 min, respectively. Reaction products were resolved by denaturing polyacrylamide gel electrophoresis. After electrophoresis, the reaction products were visualized by staining with NA-Red (Beyotime). C, quantification of the efficiencies of tRNA^{Ala} precursors catalyzed by RNase Z. The relative processing efficiencies were calculated from the initial phase of the reaction. The calculations were based on three independent determinations. The error bars indicate two standard errors of the mean (SEM).

other clinical abnormalities, including cardiac failure, muscular diseases, visual failure, and neurological disorders. Further analysis showed that the m.5587A>G mutation was present in homoplasmy in all matrilineal relatives but not in other members of these families (data not shown).

The aberrant 3' end processing of tRNA^{Ala} precursors

To examine whether the m.5587A>G mutation altered the 3' end processing of tRNA^{Ala} precursor, we performed an *in vitro* processing experiment using RNase Z that was reconstituted from purified recombinant proteins ELAC2 as described previously (16). As illustrated in Figure 1A, the wild-type and mutant tRNA^{Ala} precursors corresponding to mtDNA at positions 5567 to 5655 were prepared by *in vitro* transcription, respectively. To analyze the *in vitro* processing kinetics, the wild-type and mutant tRNA^{Ala} precursors were incubated with RNase Z at various time courses. The relative processing efficiencies were calculated by the ratios of cleaved pre-tRNAs at the initial phase of reaction according to the fitted curve under exponential equation (one-phase association). As shown in Figure 1B, the processing efficiencies of the mutant tRNA^{Ala} transcripts were significantly reduced, as compared with those of wild-type counterparts. As shown in Figure 1C, the processing efficiencies of mutant tRNA^{Ala} transcripts catalyzed by RNase Z were 44.2% of those in their wild-type counterparts, respectively. These results demonstrated that the m.5587A>G mutation perturbed the 3' end processing of tRNA^{Ala} precursors.

Impairment of 3' CCA-adding activity of tRNA^{Ala}

To assess whether the m.5587A>G mutation impaired the CCA-adding activity of tRNA^{Ala}, we performed an *in vitro* processing experiment using a CCA-adding enzyme TRNT1 (16, 45, 46). As shown in Figure 2A, the wild-type and mutant tRNA^{Ala} without the 3'-terminal CCA sequences corresponding to mtDNA at positions 5587 to 5655 were prepared by *in vitro* transcription and their capability of incorporating CCA catalyzed by the recombinant TRNT1 was then evaluated, respectively (17). To analyze the *in vitro* processing kinetics, the wild-type and mutant tRNA^{Ala} precursors were incubated with TRNT1 at various time courses. The relative processing efficiencies were calculated by the ratios of added CCA tail at the initial phase of reaction. As shown in Figure 2, B and C, the 3' end CCA-adding activities in the mutant transcripts were 57.9% of those in their wild-type counterparts, respectively. These results revealed that the m.5587A>G mutation inhibited the activity of CCA-adding of tRNA^{Ala} catalyzed by TRNT1.

Altered conformation and stability of tRNA^{Ala}

It was anticipated that the m.5587A>G mutation caused the structural alteration and instability of tRNA^{Ala}. To experimentally test the effect of m.5877A>G mutation on the stability of tRNA^{Ala}, we examined the melting temperatures (T_m) of wild-type (A73) and mutant (G73) tRNA^{Ala} transcripts. These T_m values were determined by calculating the

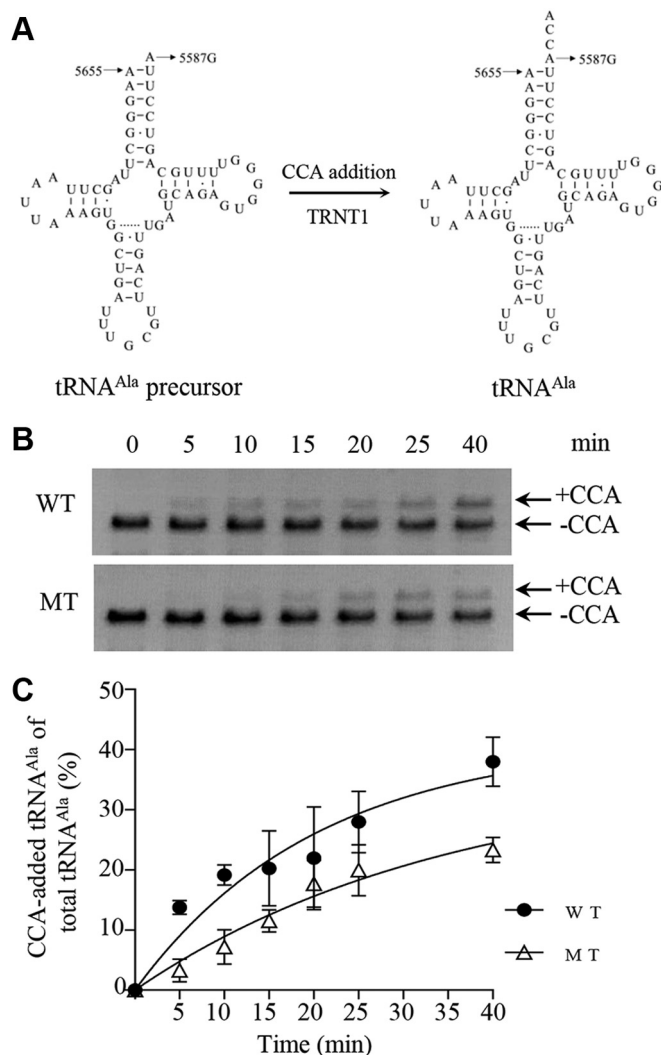


Figure 2. *In vitro* analysis for the CCA-adding activity of mitochondrial tRNA^{Ala}. A, the wild-type and mutant tRNA^{Ala} without the 3'-terminal CCA sequences were prepared by *in vitro* transcription and their capability of incorporating CCA was analyzed by the recombinant TRNT1. Mitochondrial tRNA^{Ala} precursors. B, *in vitro* analysis for the CCA-adding activity. Assays for the CCA-adding activity with CCA-adding enzyme TRNT1 were carried out in parallel for wild-type and mutant substrates. Samples were withdrawn and stopped after 5, 10, 15, 20, 25, or 40 min, respectively. Reaction products were resolved by denaturing polyacrylamide gel electrophoresis. After electrophoresis, the reaction products were visualized by staining with NA-Red (Beyotime). C, quantification of the efficiencies of tRNA^{Ala} precursors catalyzed by RNase Z. The relative processing efficiencies were calculated from the initial phase of the reaction. The calculations were based on three independent determinations. The error bars indicate two SEM.

derivatives of the absorbance against a temperature curve (47). As shown in Figure 3A, the T_m values for wild-type (A73) and mutant (G73) transcripts were $33.6 \text{ }^\circ\text{C} \pm 0.7 \text{ }^\circ\text{C}$ and $39.6 \text{ }^\circ\text{C} \pm 0.7 \text{ }^\circ\text{C}$, respectively. These results suggested that tRNA^{Ala} molecule with G37 may be more stable than tRNA^{Ala} with A37.

To test if the m.5587A>G mutation affected the conformation of tRNA^{Ala} *in vivo*, total RNAs isolated from mutant and control cell lines were electrophoresed through 10% native gel and then electroblotted onto a positively charged nylon membrane for hybridization analysis with oligodeoxynucleotide

Mechanism for mitochondrial tRNA 3'-end deficiency

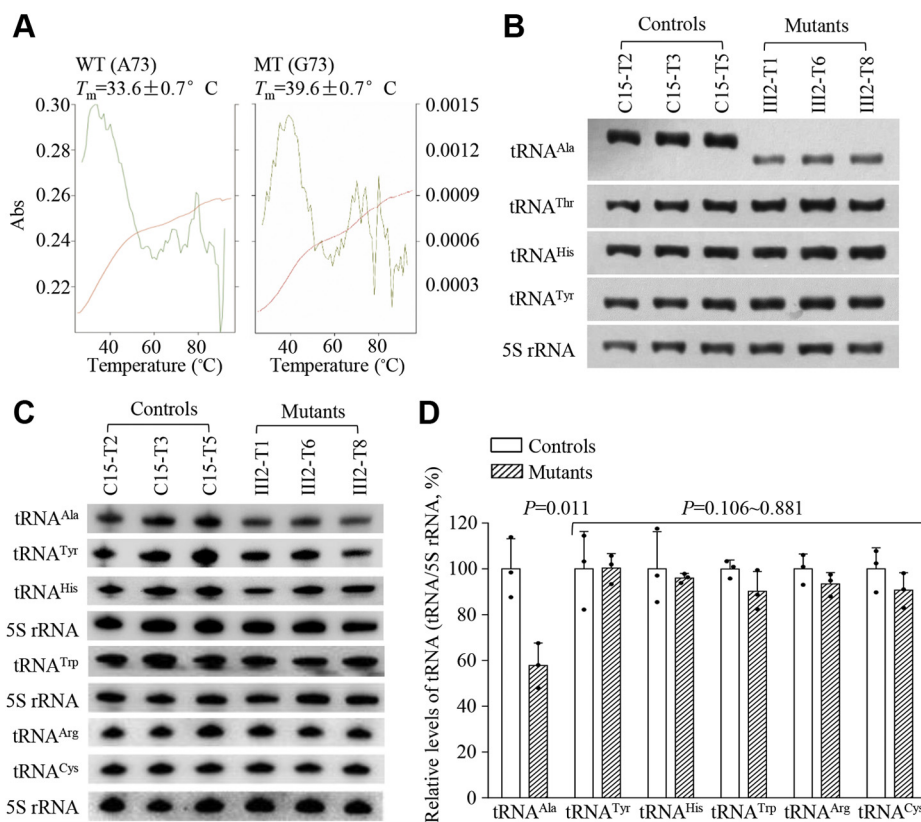


Figure 3. In vitro analysis for conformation and stability of tRNA^{Ala}. A, melting profiles of WT and MT tRNA^{Ala} transcripts measured at 260 nm with a heating rate of 1°/min from 25 to 95°. First derivative (dA/dT) against temperature curves was shown to highlight the T_m value transitions. B, northern blot analysis of tRNAs under native conditions. Ten micrograms of total cellular RNA from various cell lines was electrophoresed through native polyacrylamide gel, electroblotted, and hybridized with DIG-labeled oligonucleotide probes specific for the tRNA^{Ala}, tRNA^{Thr}, tRNA^{His}, tRNA^{Tyr}, and 5S rRNA, respectively. C, northern blot analysis of tRNA under denaturing condition. Ten micrograms of total cellular RNAs from the various cell lines was electrophoresed through a 10% denaturing polyacrylamide gel, electroblotted, and hybridized with DIG-labeled oligonucleotide probes specific for tRNA^{Ala}, other five tRNAs and 5S rRNA, respectively. D, quantification of tRNA levels. Average relative each tRNA content per cell was normalized to the average content per cell of 5S rRNA in the control and mutant cybrids, respectively. The values for the latter were expressed as percentages of the average values for the control cybrids. The calculations were based on three independent determinations in each cybrids. The error bars indicate two SEM. P indicates the significance, according to the t -test, of the difference between mutant and control cybrids.

probes for tRNA^{Ala}, tRNA^{Thr}, tRNA^{His}, and tRNA^{Tyr}, respectively (47). As shown in Figure 3B, electrophoretic patterns showed that the tRNA^{Ala} in three mutant cybrid cell lines carrying the m.5587A>G mutation migrated faster than those of control cybrid cell lines lacking this mutation. These data indicated the m.5587A>G mutation resulted in the conformation change of tRNA^{Ala}.

Reductions in the steady-state levels of tRNA^{Ala}

To further assess if the m.5587A>G mutation ablated the stability of tRNA^{Ala}, we subjected mitochondrial RNAs from mutant and control cybrids to Northern blots through 10% denature gel and hybridized them with DIG-labeled oligodeoxynucleotide probes for 22 tRNAs and 5S rRNA as the loading control (7, 31). As shown in Figure 3C, the steady-state level of tRNA^{Ala} in the mutant cells was markedly decreased, as compared with those in control cells. For comparison, the average levels of each tRNA in the various control or mutant cybrids were normalized to the average levels in the same cell lines for reference 5S rRNA. As shown in Figure 3D, the average level of tRNA^{Ala} in the mutant cybrid cell lines was

57.83% ($p = 0.011$) of those in control cell lines, respectively. However, the average levels of other 21 tRNAs in three mutant cybrids were comparable with those in three control cybrids (Fig. 3, C and D, Fig. S2).

Deficient aminoacylation of tRNA^{Ala}

The A73 is the discriminator base for its cognate aminoacyl-tRNA synthetase (42). To evaluate if the m.5587A>G mutation affected the aminoacylation of tRNA, we examined the aminoacylation levels of tRNA^{Ala}, tRNA^{Thr}, tRNA^{His}, and tRNA^{Tyr} by the use of electrophoresis in an acidic urea PAGE system to separate uncharged tRNA species from the corresponding charged tRNA, electroblotting and hybridizing with the tRNA probes as described above (47, 48). As shown in Figure 4A, the upper band represents the charged tRNA, and the lower band represents uncharged tRNA. The electrophoretic mobility of either charged or uncharged tRNA^{Ala} in the mutant cell lines migrated faster than those of control cell lines. To further distinguish nonaminoacylated tRNA from aminoacylated tRNA, samples of tRNAs were deacylated by being heated for 10 min at 60 °C (pH 8.3) and then run in

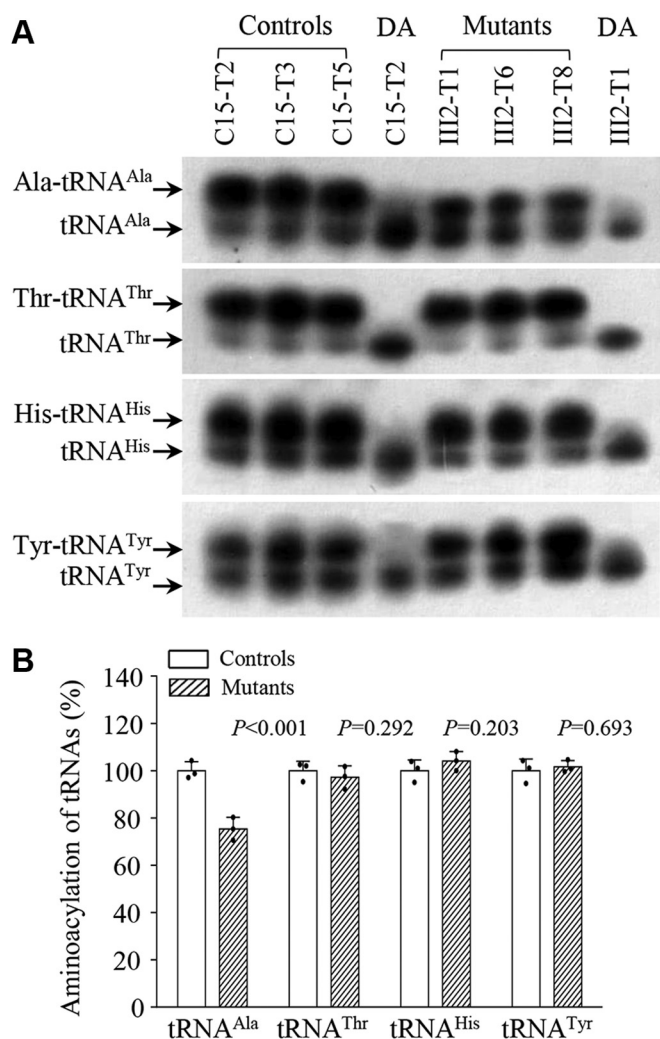


Figure 4. *In vivo* aminoacylation assays. *A*, ten micrograms of total cellular RNA purified from six cell lines under acid conditions was electrophoresed at 4 °C through an acid (pH 5.0) 10% polyacrylamide-8 M urea gel, electroblotted, and hybridized with a DIG-labeled oligonucleotide probe specific for the tRNA^{Ala}. The blots were then stripped and rehybridized with tRNA^{Thr}, tRNA^{His}, and tRNA^{Tyr}, respectively. The samples from one control (C15-T2) and mutant (III2-T1) cell lines were deacylated (DA) by heating for 10 min at 60 °C at pH 8.3 and electrophoresed as above. Aminoacylation assays for tRNA^{Ala} were carried out in parallel for aminoacylated and deacylated samples. *B*, *in vivo* aminoacylated proportions of tRNAs in the mutant and controls. The calculations were based on three independent determinations. Graph details and symbols are explained in the legend to the Figure 3.

parallel. Only one band (uncharged tRNA) was present in both mutant and control cell lines after deacylating. However, there were no obvious differences in electrophoretic mobility of tRNA^{Thr}, tRNA^{His}, and tRNA^{Tyr}. As shown in Figure 4B, the efficiencies of aminoacylated tRNA^{Ala} in three mutant cell lines were 75.4% ($p < 0.001$) relative to the average values of three control cell lines. However, the levels of aminoacylation in tRNA^{Thr}, tRNA^{His}, and tRNA^{Tyr} in mutant cell lines were comparable with those in the control cell lines.

Decreases in the levels of mitochondrial proteins

To investigate whether the m.5587A>G mutation impaired mitochondrial translation, western blot analysis was carried

out to examine the steady-state levels of 11 mtDNA-encoded polypeptides [ND1, ND3, ND4, ND5, and ND6 (subunits 1, 3, 4, 5, and 6 of NADH dehydrogenase), CYTB (apocytocrome b), CO1, CO2, CO3 (subunits I, II, and III of cytochrome c oxidase), and ATP6, ATP8 (ATPase)] in mutant and control cybrids with GAPDH as a loading control. As shown in Figure 5, *A* and *B*, the overall levels of 11 mtDNA-encoded polypeptides in the mutant cell lines were 69.8% ($p < 0.001$), relative to the mean values measured in the control cell lines. The average levels of ND1, ND3, ND4, ND5, ND6, CO1, CO2, CO3, CYTB, ATP6, and ATP8 in three mutant cybrids were 66.4%, 74%, 55.1%, 65.1%, 73%, 81.5%, 63%, 70%, 52.4%, 66.8%, and 100.9% of those in three control cybrids after normalization to GAPDH, respectively. As shown in Table S2, the reduced levels among 11 mtDNA-encoding polypeptides in the mutant cybrids bearing the 5587A>G mutations were correlated with the proportion of alanine in the polypeptides.

Deficient activities of respiratory chain complexes

To evaluate the effect of the m.5587A>G mutation on the oxidative phosphorylation, we measured the activities of respiratory complexes by the use of isolating mitochondria from mutant and control cell lines. The activity of complex I (NADH ubiquinone oxidoreductase) was determined through the oxidation of NADH with ubiquinone as the electron acceptor (49). Complex II (succinate ubiquinone oxidoreductase) was examined by the activity of complex II through the artificial electron acceptor DCPIP. The activity of complex III (ubiquinone cytochrome c oxidoreductase) was measured through the reduction of cytochrome c (III) by using D-ubiquinol-2 as the electron donor. The activity of complex IV (cytochrome c oxidase) was monitored through the oxidation of cytochrome c (II). As shown in Figure 6A, the activity of complexes I, III, and IV in three mutant cybrids carrying the m.5587A>G mutation were 71.2% ($p = 0.006$), 85.1% ($p = 0.013$), and 77.6% ($p = 0.008$) of the mean values measured in three control cybrids, respectively, while the activity of complex II in three mutant cybrids carrying the m.5587A>G mutation was 107.1% ($p = 0.388$) of the mean values measured in three control cybrids.

We then measured oxygen consumption rates (OCR) of various mutant and control cell lines using Seahorse Bioscience XF-96 Extracellular Flux Analyzer (50). As shown in Figure 6, *B* and *C*, the basal OCR in three mutant cell lines was 73.9% ($p = 0.008$) relative to the mean values measured in three control cell lines. To investigate which of the enzyme complexes of the respiratory chain was affected in the mutant cell lines, oligomycin (to inhibit the ATP synthase), carbonyl cyanide 4-trifluoromethoxy-phenylhydrazone (FCCP) (to uncouple the mitochondrial inner membrane and allow for maximum electron flux through the ETC), rotenone (to inhibit complex I), and antimycin A (to inhibit complex III) were added sequentially while measuring OCR. The difference between the basal OCR and the drug-insensitive OCR yields the

Mechanism for mitochondrial tRNA 3'-end deficiency

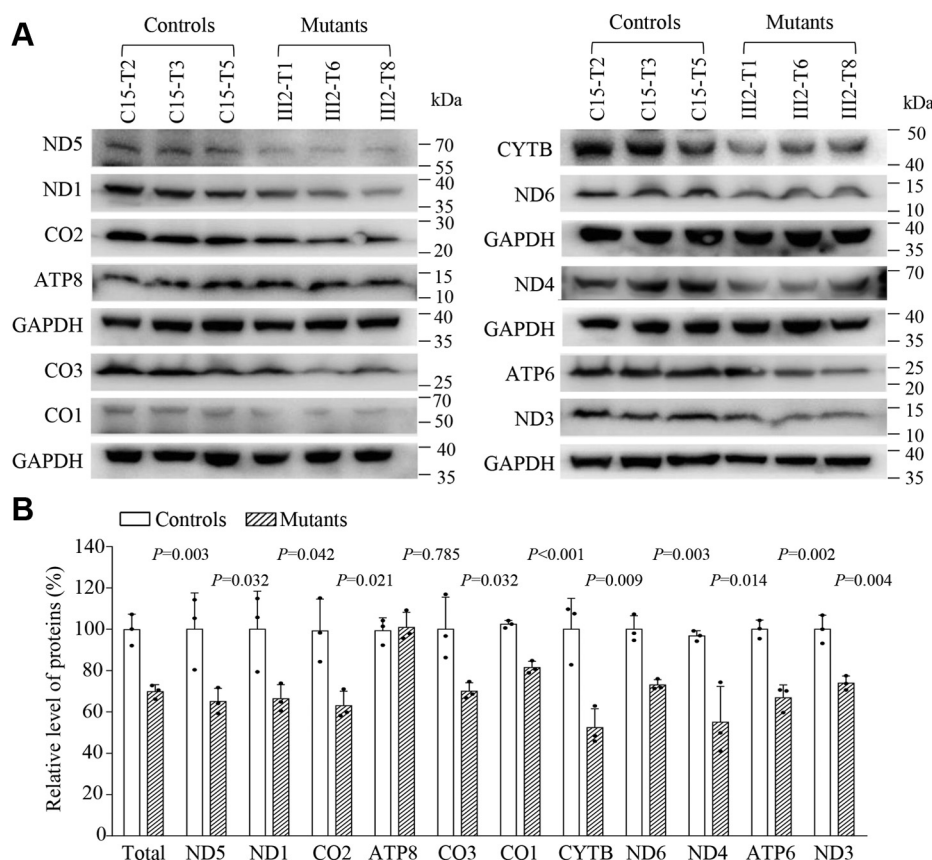


Figure 5. Analysis of mitochondrial proteins. A, twenty micrograms of total cellular proteins from various cell lines was electrophoresed through a denaturing polyacrylamide gel, electroblotted, and hybridized with 11 mtDNA encoding polypeptides in mutant and control cells with GAPDH as a loading control. B, quantification of mitochondrial protein levels. Average relative ND1, ND3, ND4, ND5, ND6, CO1, CO2, CO3, ATP8, ATP6, and CYTB content per cell, normalized to the average content per cell of GAPDH in three mutant cell lines carrying the m.5587A>G mutation and three control cell lines lacking the mutation. The values for the latter are expressed as percentages of the average values for the control cell line. The calculations were based on three independent determinations. Graph details and symbols are explained in the legend to Figure 3.

amount of ATP-linked OCR, proton leak OCR, maximal OCR, reserve capacity, and nonmitochondrial OCR. As shown in Figure 6, B and C, the ATP-linked OCR, proton leak OCR, maximal OCR, reserve capacity, and nonmitochondrial OCR in three mutant cell lines were 67.5% ($p = 0.003$), 85.7% ($p = 0.328$), 74.4% ($p = 0.006$), 96.7% ($p = 0.947$), and 88.4% ($p = 0.039$), relative to the mean values measured in three control cell lines, respectively.

Instability of OXPHOS complexes

We analyzed the consequence of m.5587A>G mutation on the stability and activity of complexes I, II, and IV using the in-gel activity assay. Mitochondrial membrane proteins isolated from mutant and control cell lines were separated by blue native electrophoresis analysis (BN-PAGE) and stained with specific substrates of complexes I, II, and IV (51, 52). As illustrated in Figure 7A, mutant cybrids carrying m.5587A>G mutation exhibited defective assembly of intact super-complexes and complex I. As shown in Figure 7B, the in-gel activities of complexes I and IV in mutant cell lines carrying m.5587A>G mutation were 72% ($p = 0.004$) and 82.2% ($p < 0.001$), relative to the average values of control cell lines, respectively. In contrast, the average in-gel activities of

complexes II in the mutant cell lines were comparable with those of the control cell lines.

Reduced levels in mitochondrial ATP production

We used the luciferin/luciferase assay to examine the capacity of oxidative phosphorylation in mutant and wild-type cell lines. Populations of cells were incubated in the media in the presence of glucose and 2-deoxy-D-glucose with pyruvate (53). As shown in Figure 7C, the levels of ATP production in mutant cell lines in the presence of glucose (total cellular levels of ATP) were comparable with those measured in control cell lines. In contrast, the levels of ATP production in mutant cell lines, in the presence of 2-deoxy-D-glucose and pyruvate to inhibit the glycolysis (mitochondrial levels of ATP), varied from 68% to 75.5%, with an average of 72.1% relative to the mean values measured in the control cell lines ($p < 0.001$).

Decrease in mitochondrial membrane potential

The mitochondrial membrane potentials ($\Delta\Psi_m$) were measured through the fluorescence probe JC-10 assay system in three mutant and three control cell lines (Fig. S3) (54). The ratios of fluorescence intensities of Ex/Em = 490/590 and

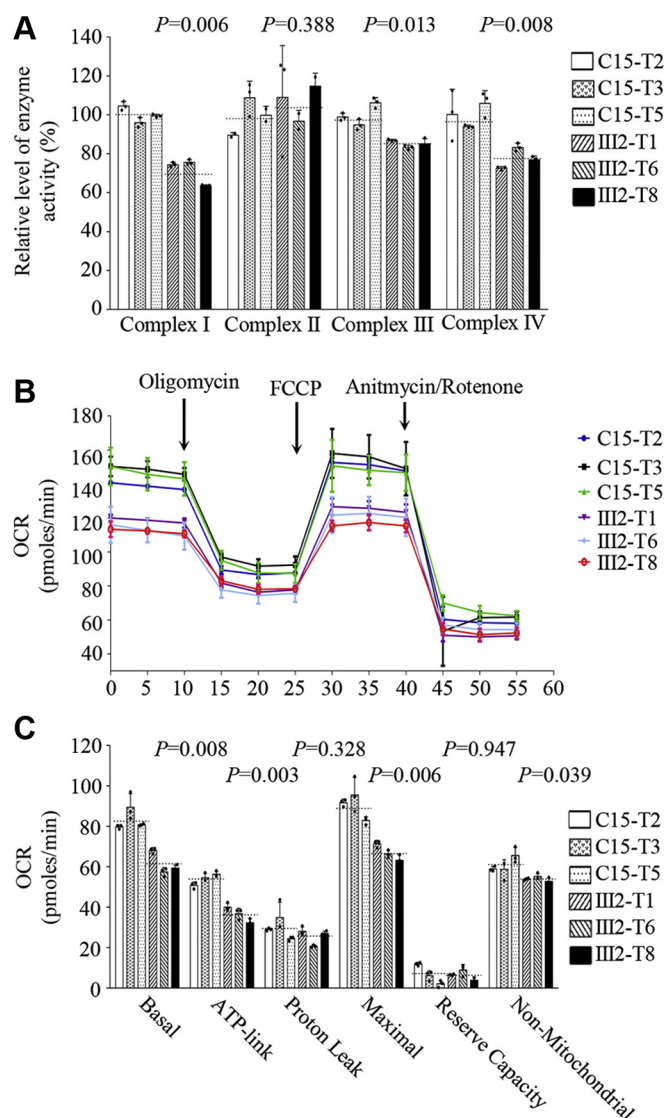


Figure 6. Analysis of enzymatic activities in the OXPHOS complex. A, the enzymatic activities of electron transport chain complexes were investigated by enzymatic assay on complexes I, II, III, and IV in isolated mitochondrial membranes from three mutant and control cybrid cell lines. B, an analysis of O_2 consumption in the various cell lines using different inhibitors. The rates of O_2 (OCR) were first measured on 2×10^4 cells of each cell line under basal condition and then sequentially added to oligomycin (1.5 μ M), FCCP (0.5 μ M), rotenone (1 μ M), and antimycin A (1 μ M) at indicated times to determine different parameters of mitochondrial functions. C, graphs presented the ATP-linked OCR, proton leak OCR, maximal OCR, reserve capacity, and nonmitochondrial OCR in mutant and control cell lines. Nonmitochondrial OCR was determined as the OCR after rotenone/antimycin A treatment. Basal OCR was determined as OCR before oligomycin minus OCR after rotenone/antimycin A. ATP-linked OCR was determined as OCR before oligomycin minus OCR after oligomycin. Proton leak was determined as basal OCR minus ATP-linked OCR. Maximal was determined as the OCR after FCCP minus nonmitochondrial OCR. Reserve capacity was defined as the difference between maximal OCR after FCCP minus basal OCR. The average of three determinations for each cell line is shown, the horizontal dashed lines represent the average value for each group. Graph details and symbols are explained in the legend to Figure 3.

490/530 nm (FL590/FL530) were recorded to delineate the $\Delta\Psi_m$ of each sample. The relative ratios of FL590/FL530 geometric mean between mutant and control cell lines were calculated to represent the level of $\Delta\Psi_m$ ⁵⁴. As shown in Figure 7D, the $\Delta\Psi_m$ of three mutant cell lines carrying the

m.5587A>G mutation ranged from 78.4% to 81.8%, with an average of 79.6% ($p < 0.001$) of the mean values measured in three control cell lines. In contrast, the levels of $\Delta\Psi_m$ in mutant cell lines in the presence of FCCP were comparable with those of control cell lines.

The increase of ROS production

Mitochondrial ROS plays a critical role in physiological consequences (55–57). We assessed ROS production in mutant and control cybrid cell lines *via* flow cytometry, comparing baseline staining intensity for each cell line with that upon oxidative stress to obtain a ratio corresponding to ROS generation (30, 52, 58). Geometric mean intensity was recorded to measure the rate of mitochondrial ROS of each sample. The relative levels of geometric mean intensity in each cell line were calculated to delineate the levels of mitochondrial ROS in mutant and control cells. As shown in Figure 8, A and B, the levels of ROS generation in the mutant cybrids carrying the m.5587A>G mutation ranged from 118.8% to 127.4%, with an average of 123.4% ($p = 0.007$) of the mean values measured in the control cell lines. Furthermore, we examined the levels of catalase and superoxide dismutase proteins (SOD2 and SOD1) in mutant and control cell lines by western blot analysis (56, 57). As shown in Figure 8, C and D, significant increasing levels of these proteins were observed in the mutant cybrids. In particular, the average levels of catalase, SOD2, and SOD1 in three mutant cell lines carrying the m.5587A>G mutation were 123.7%, 133.4%, and 133%, relative to the mean values measured in three control cell lines, respectively.

Promoting apoptosis

Deficient activities of oxidative phosphorylation have been linked to protection against certain apoptotic stimuli (58, 59). To evaluate if the m.5587A>G mutation affected the apoptotic processes, we examined the apoptotic state of mutant and control cybrids by immunofluorescence and western blot analyses. As shown in Figure 9A, the immunofluorescence patterns of double-labeled cells with rabbit monoclonal antibody specific for the cytochrome c and mouse monoclonal antibody to TOM20 revealed markedly increased levels of cytochrome c in the mutant cells, compared with control cells. The levels of cytochrome c in cytosol in mutant and control cell lines were further evaluated by western blot analysis. As shown in Figure 9, B and C, the levels of cytochrome c in three mutant cell lines ranged from 120.7% to 154.3%, with an average of 141.9% ($p = 0.021$), relative to the average values in three control cell lines. Furthermore, we examined the levels of four apoptosis activated proteins [caspases 3, 9 and Poly ADP ribose polymerase (PARP)] in mutant and control cell lines by western blot analysis (59, 60). The average levels of caspases 3, 9 and PARP in three mutant cell lines were 119.3% ($p = 0.006$), 143% ($p = 0.003$), and 119.7% ($p = 0.018$) of the average values measured in three control cell lines, respectively.

Mechanism for mitochondrial tRNA 3'-end deficiency

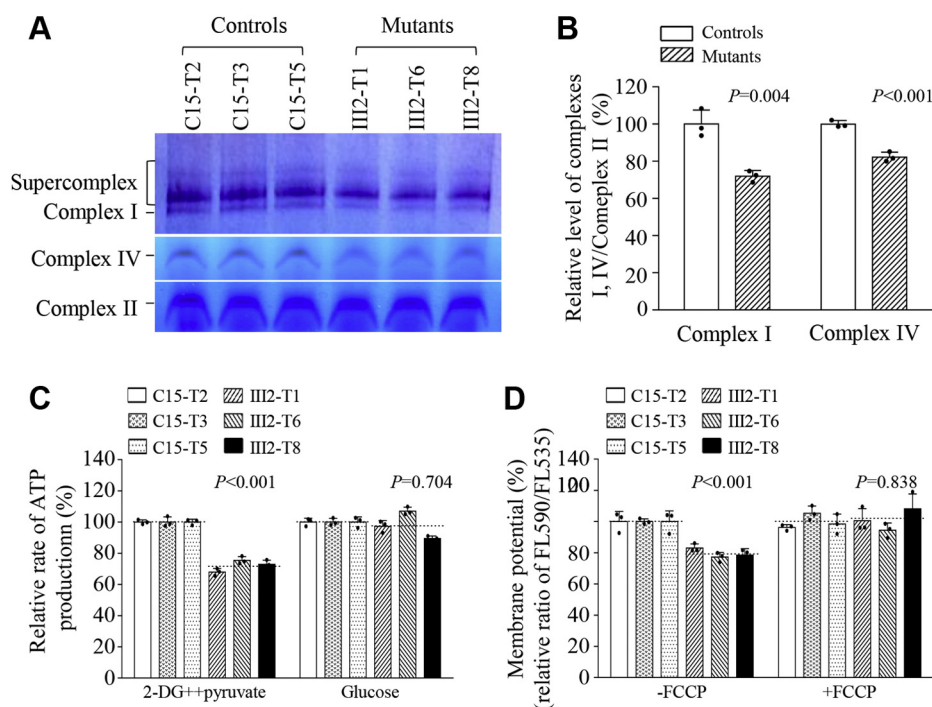


Figure 7. BN-PAGE analysis of OXPHOS complexes, measurement of ATP levels and membrane potential. *A*, in-gel activity of complexes I, II, and IV. Twenty micrograms of mitochondrial proteins from various mutant and control cell lines was used for BN-PAGE, and the activities of complexes were measured in the presence of specific substrates (NADH and NTB for complex I, sodium succinate, phenazine methosulfate, and NTB for complex II, and DAB and cytochrome c for complex IV). *B*, quantification of in-gel activities of complexes I, II, and IV. The calculations were based on three independent determinations in each cell line. *C*, measurement of cellular and mitochondrial ATP levels using bioluminescence assay. ATP levels from mutant and control cell lines were measured using a luciferin/luciferase assay. Mutant and control cell lines were incubated with 10 mM glucose or 5 mM 2-deoxy-D-glucose plus 5 mM pyruvate to determine ATP generation under mitochondrial ATP synthesis. Average rates of ATP level per cell line in mitochondria are shown. *D*, mitochondrial membrane potential analysis. The mitochondrial membrane potential ($\Delta\Psi_m$) was measured in mutant and control cell lines using a fluorescence probe JC-10 assay system. The ratio of fluorescence intensities $Ex/Em = 490/590$ nm and $490/530$ nm (FL_{590}/FL_{530}) was recorded to delineate the $\Delta\Psi_m$ level of each sample. The relative ratios of FL_{590}/FL_{530} geometric mean between m.5587A>G mutation and control cell lines were calculated to reflect the level of $\Delta\Psi_m$. Relative ratio of JC-10 fluorescence intensities at $Ex/Em = 490/525$ and $490/590$ nm in the absence and presence of 10 μ M of FCCP in three control cell lines and three mutant cell lines. The average of three determinations for each cell line is shown. Graph details and symbols are explained in the legend to Figure 3.

Alteration in mitophagy

Mitophagy is the selective removal of damaged mitochondria by autophagosomes and their subsequent catabolism by lysosomes (61–63). To investigate if the m.5587A>G mutation affected the mitophagy, we evaluated the mitophagic states of mutant and control cell lines using endogenous immunofluorescence and western blotting assays. As shown in Figure 10A, mutant cell lines displayed reduced levels of LAMP1 (lysosome-associated membrane glycoprotein 1), indicating that the m.5587A>G impaired the mitophagy process (61). The status of mitophagy in mutant and control cell lines was then examined using western blot analysis using two markers: microtubule-associated protein 1A/1B light-chain 3B (LC3) and sequestosome 1 (SQSTM1/p62) (62, 63). During autophagy, the cytoplasmic form (LC3-I) is processed into a cleaved and lipidated membrane-bound form (LC3-II), which is essential for membrane biogenesis and closure of the membrane. LC3-II is recycled by cysteine protease (Atg4B) following completion of the autophagosome and recycled. SQSTM1/p62, one of the best-known autophagic substrates, interacts with LC3 to ensure the selective delivery of these proteins into the autophagosome (63). As shown in Figure 10, B and C, the reduced levels of

LC3 and increased levels of p62 were observed in the mutant cybrids carrying the m.5587A>G mutation, compared with those in the control cybrids. In particular, the average levels of LC3-II/(LC3-I+II) and p62 in three mutant cell lines carrying the m.5587A>G mutation were 162.5% ($p = 0.001$) and 66.1% ($p = 0.002$) of the mean values measured in three control cell lines lacking the mutation, respectively. These data suggested that the m.5587A>G mutation promoted the mitophagy in mutant cybrids.

Discussion

LHON is the most common type of maternally transmitted eye disorder and is characterized by the degeneration of retinal ganglion cells (RGC) and loss of central vision (64). In the majority of cases worldwide, LHON was caused by three primary mtDNA point mutations: ND4 11778G>A, ND6 14484T>C, and ND1 3460G>A, affecting subunits of complex I (64–68). In the present study, we investigated the pathophysiology of the first LHON-linked tRNA mutation: tRNA^{Ala} 5587A>G mutation. This mutation was only present in the matrilineal relatives of three Chinese families with suggestive maternal inheritance of LHON. The occurrence of m.5587A>G mutation in these genetically unrelated pedigrees

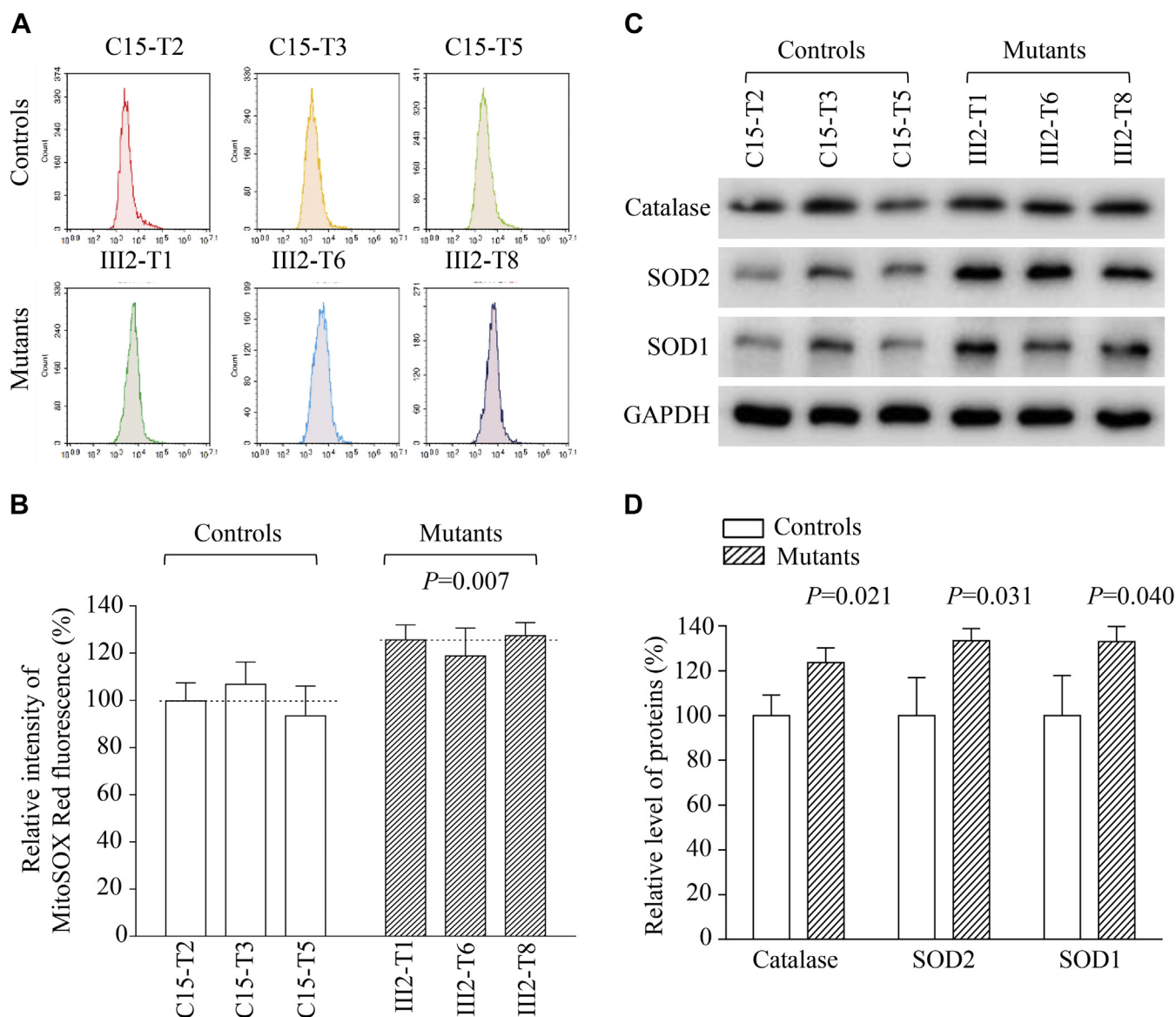


Figure 8. Analysis of mitochondrial ROS production. A and B, the rates of ROS generation by mitochondria in living cells from mutant and control cell lines were analyzed by a Novocyte flow cytometer (ACEA Biosciences) using the mitochondrial superoxide indicator MitoSOX-Red (5 mM). A, flow cytometry histogram showing MitoSOX-Red fluorescence of various cell lines. B, relative ratios of MitoSOX-Red fluorescence intensity. The average of three determinations for each cell line is shown. C, western blot analysis of three antioxidative enzymes. Twenty micrograms of total cellular proteins from various cell lines was electrophoresed, electroblotted, and hybridized with catalase, SOD1, and SOD2 antibodies and with GAPDH as a loading control. D, quantification of SOD2, SOD1, and catalase. Average relative values of SOD2, SOD1, and catalase were normalized to the average values of GAPDH in various cell lines. The values for the latter are expressed as percentages of the average values for the control cell lines. The average of three independent determinations for each cell line is shown. Graph details and symbols are explained in the legend to Figure 3.

affected by LHON and differing considerably in their mtDNA sequences strongly indicated that this mutation is involved in the pathogenesis of LHON (39). It was anticipated that the m.5587A>G mutation altered the structure and function of tRNA^{Ala}. The *in silico* analysis suggested that the m.5587A>G mutation resulted in an alternate secondary structure fold of the tRNA transcript (69). The altered structure of tRNA^{Ala} caused by the m.5587A>G mutation was evidenced by the increased melting temperature of mutated tRNA with respect to the wild-type molecule *in vitro* transcripts, as in the case of tRNA^{His} U68>C68 and tRNA^{Ala} A1>G1 mutations (30, 53). The potentially altered structure of tRNA^{Ala} was responsible

for the differential tRNA migration on native gels of mutated tRNA with respect to the wild-type molecule *in vitro* or *ex vivo*.

Here, we demonstrated that the m.5587A>G mutation had pleiotropic effects on the maturation of tRNA^{Ala}. The primary defect arising from the m.5587A>G mutation was the aberrant 3' end processing of tRNA^{Ala} from the L-strand transcripts harboring the ND6 and eight tRNAs including tRNA^{Ala} (7, 13, 14). The tRNA processing defects were evidenced by reduced efficiencies of the 3' end processing of tRNA^{Ala} precursors carrying the m.5587A>G mutation using *in vitro* processing assay and decreased levels of tRNA^{Ala} observed in the mutant cells bearing

Mechanism for mitochondrial tRNA 3'-end deficiency

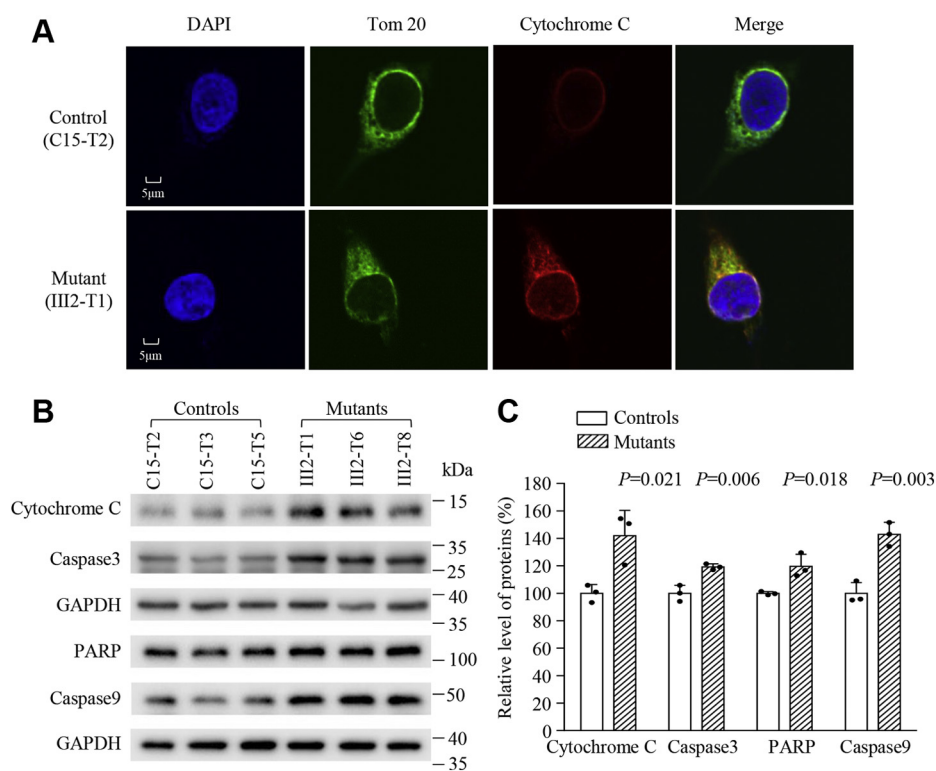


Figure 9. Analysis of apoptosis. A, the distributions of cytochrome c from cybrids (III2-T1 and C15-T2) were visualized by immunofluorescent labeling with TOM20 antibody conjugated to Alex Fluor 488 (green) and cytochrome c antibody conjugated to Alex Fluor 594 (red) analyzed by confocal microscopy. DAPI-stained nuclei were identified by their blue fluorescence. B, western blot analysis of cytochrome c and three apoptosis-activated proteins. Twenty micrograms of total proteins from various cell lines were electrophoresed, electroblotted, and hybridized with cytochrome c, caspases 9 and 3, and PARP antibodies, with GAPDH as a loading control. C, quantification of cytochrome c and three apoptosis-activated proteins. Three independent determinations were done in each cell line. Graph details and symbols are explained in the legend to Figure 3.

the m.5587A>G mutation. By contrast, the m.5587A>G mutation did not affect the processing of 14 tRNAs, which are cotranscribed from the L-strand mtDNA, and other seven tRNAs, which are cotranscribed from the H-strand mtDNA (7, 13, 14, 31). Addition of CCA triplet to the 3' end of mitochondrial tRNAs catalyzed by the enzyme TRNT1 is an important step in the tRNA maturation process and essential for translation (17–19). Here, we showed that the m.5587A>G mutation significantly inhibited the CCA addition of tRNA^{Ala} catalyzed by TRNT1. In fact, the substitution of C72 with U72 in the tRNA^{Leu(UUR)} by m.3303C>T mutation led to a significant effect on CCA addition of this tRNA (33). Furthermore, the discriminator base A73 at the acceptor stem of tRNA^{Ala} is critical for its specific recognition by cognate aminoacyl-tRNA synthetase (40–42, 70–72). The *in vitro* aminoacylation assays showed the complete loss of alanylation of tRNA^{Ala} mutants with U73 or C73 and marked decreases in alanylation of tRNA^{Ala} mutant with G73 (27). The impact of purine bases at position 73 on alanylation was further supported by the fact that the cell lines bearing the m.5587A>G mutation exhibited reduced efficiency of tRNA^{Ala} aminoacylation in the mutant cell lines and faster electrophoretic mobility of mutated tRNA with respect to the wild-type molecules. Indeed, the faster electrophoretic mobility observed in both native and acid conditions was likely due to a defect of tRNA maturation caused by the m.5587A>G mutation. As a result, deficiencies in the tRNA^{Ala} 3' end metabolism then contributed to the lower levels of tRNA^{Ala} in

the cybrids carrying the m.5587A>G mutation under native and denatured conditions. However, ~42% reduction in the steady-state level of tRNA^{Ala} in mutant cybrids carrying the m.5587A>G mutation was above the proposed threshold level (70% reduction) to produce a clinical phenotype (35, 53, 73). Therefore, the m.5587A>G mutation may be the primary causative evident but itself insufficient to produce the clinical phenotype.

The m.5587A>G mutation-induced ramifications of tRNA^{Ala} metabolisms impaired the synthesis of 13 mtDNA encoding proteins. In the present study, mutant cell lines carrying the m.5587A>G mutation exhibited the variable reductions (average of 30%) in the levels of 11 mtDNA-encoded polypeptides, ranging from sharp reductions (48%) in the levels of CYTB to no reduction of ATP8. Notably, the reduced levels of these polypeptides in mutant cybrids were significantly correlated with the proportions but not number of alanines (Table S2), consistent with what was previously shown in cells carrying the tRNA^{Ser(UCN)} 7445A>G mutation (35). The impairment of mitochondrial protein synthesis perturbed the stabilities and activities of OXPHOS complexes in the mutant cells bearing the m.5587A>G mutation. In particular, impaired synthesis of complex I subunits (ND1, ND3 ND4, ND5, and ND6) and complex IV subunits (CO1, CO2, and CO3) contributed to the deficiencies in the assembly and activity of complexes I and complex IV, respectively.

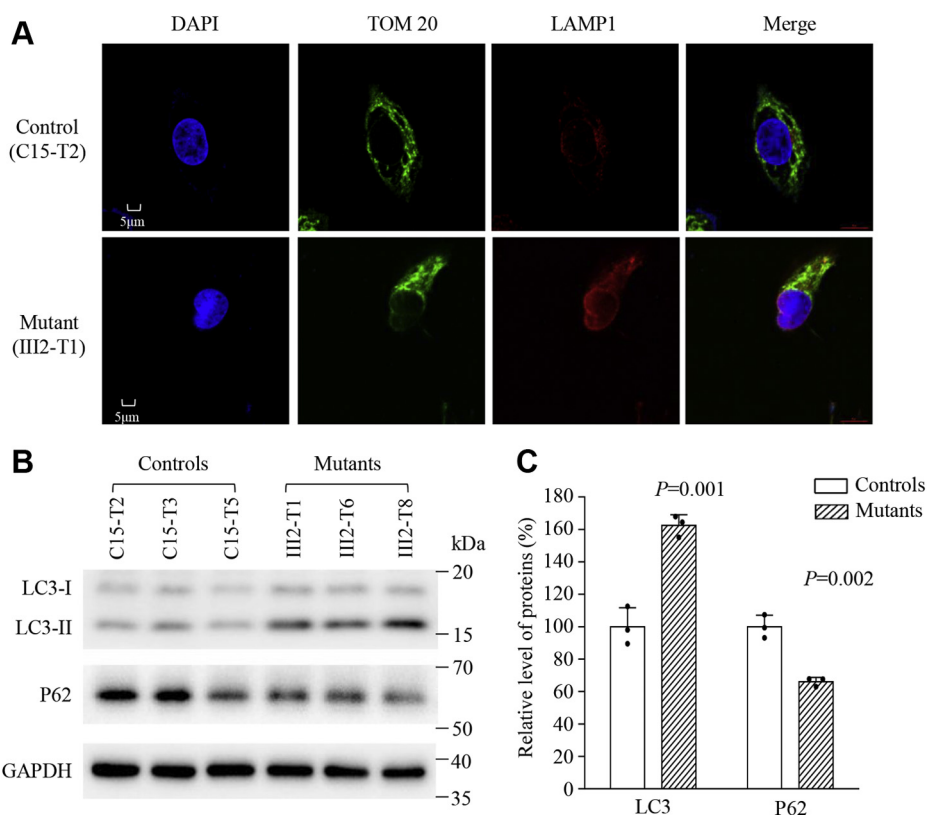


Figure 10. Assessment of autophagy. *A*, the distributions of LAMP1 from mutant (III2-T1) and control (C15-T2) cell lines were visualized by immunofluorescent labeling with TOM20 antibody conjugated to Alex Fluor 488 (green) and LAMP1 antibody conjugated to Alex Fluor 594 (red) analyzed by confocal microscopy. DAPI-stained nuclei were shown by the blue fluorescence. *B*, western blot analysis for autophagic response protein LC3-I/II and p62. Twenty micrograms of total cellular proteins from various cell lines was electrophoresed, electroblotted, and hybridized with LC3 and p62 antibodies and with β -actin as a loading control. *C*, quantification of autophagy markers LC3A/B and p62 in the mutant cell lines and control cell lines. Graph details and symbols are explained in the legend to Figure 3.

Furthermore, the m.5587A>G mutation-induced oxidative phosphorylation deficiencies were further supported by significant decreases in the basal OCR, ATP-linked OCR, and maximal OCR as well as significant reductions in the level of mitochondrial ATP in mutant cell lines carrying the m.5587A>G mutation, as revealed by those in the cell lines carrying the tRNA^{Asp} 7551A>G, tRNA^{Met} 4435A>G, and tRNA^{Ile} 4295A>G mutations (23, 47, 74). As a result, the defective oxidative phosphorylation diminished mitochondrial membrane potentials and elevated the production of ROS and the subsequent failure of cellular energetic processes (75). In particular, the effect of ROS overproduction on cellular functions was evidenced by the increasing expression of antioxidant enzymes SOD1, SOD2 and catalase observed in the cells bearing m.5587A>G mutation (56, 76). In particular, RGCs are the biggest ATP demand cells in the retina (77, 78). Therefore, the retinal ganglion cells carrying m.5587A>G mutation may be preferentially involved because they are high ATP demand cells and somehow exquisitely sensitive to subtle imbalance in cellular redox state or increased level of free radicals (76, 79, 80).

Mitochondrial dysfunction affected the apoptotic sensitivity and mitophagy of cells carrying the LHON-associated mtDNA mutations (44, 59, 81). In the present investigation, mutant cybrids bearing the m.5587A>G mutation exhibited more

apoptotic susceptibility than control cybrids lacking the mutation. These were evidenced by the elevated releases of cytochrome c into cytosol and increased levels of apoptosis-activated proteins: caspases 9, 3 and PARP in the cybrids carrying the m.5587A>G mutation, as compared with control cybrids. These data demonstrated that m.5587A>G mutation elevated the apoptosis. Mitophagy regulates mitochondrial energy metabolism by controlling the amount and efficiency of the mitochondrial metabolic machinery (81). In particular, the impairment of OXPHOS and alteration of mitochondrial membrane potential affected the mitophagic removal of damaged mitochondria (82). The activation of mitophagic machinery is crucial to the complete degradation of mitochondrial components (83). In the present investigation, we analyzed the effect of m.5587A>G mutation on mitophagy by western blot and endogenous immunofluorescence experiments. The mutant cybrids bearing the m.5587A>G mutation displayed the increasing levels of autophagy. Furthermore, the mutant cybrids harboring the m.5587A>G mutation revealed the decreased levels of p62, which indicated the preferential reduction of autophagic substrates, and increased levels of LC3-II that implied the increasing generation of autophagosome. These data indicated that the m.5587A>G mutation promoted the autophagic degradation of ubiquitinated proteins.

Mechanism for mitochondrial tRNA 3'-end deficiency

However, the incomplete penetrance of LHON and relatively mild biochemical defects indicated that the m.5587A>G mutation is a primary factor underlying the development of LHON but is itself insufficient to produce a clinical phenotype. The other genetic or epigenetic factors may contribute to the development of clinical phenotype in the subjects carrying the m.5587A>G mutation (44, 59, 84, 85). In particular, the vision-specific phenotypes of this tRNA mutation may be attributed to the tissue specificity of OXPHOS *via* RNA maturation or involvement of nuclear modifier genes (52, 86, 87). However, the m.5587A>G mutation is also associated with Leigh syndrome, which most commonly presents as a progressive dysfunction of the central nervous system (88). Changes in RNA maturation profiles may specify cellular metabolic states and efficiently adapt protein synthesis rates to cell stress in the different tissues (24). Alternatively, the tissue heterogeneity may arise from differential expression of tRNA genes, variable activation of the integrated stress response pathway, metabolic changes, and the ability of certain tissues to respond to impaired mitochondrial translation (89, 90).

In summary, our findings convincingly demonstrate the pathogenic mechanism underlying the LHON-associated tRNA^{Ala} 5587A>G mutation. The m.5587A>G mutation led to pleiotropic effects on the 3' end processing of transcript precursor, CCA addition, aminoacylation, and stability of tRNA^{Ala}. The m.5587A>G mutation-induced ramifications of tRNA^{Ala} metabolism resulted in the decreased synthesis of mtDNA encoding polypeptides and perturbed the assembly and activity of OXPHOS. As a result, this respiratory deficiency gave rise to the decrease of mitochondrial ATP production, mitochondrial membrane potential, and the increasing production of oxidative reactive species. All those alterations consequently elevated the apoptotic cell death and promoted the mitophagy in cells carrying the m.5587A>G mutation, thereby contributing to visual loss. However, the tissue specificity of this pathogenic mtDNA mutation is likely due to the involvement of nuclear modifier genes or tissue-specific differences in tRNA metabolism. Thus, our findings may provide the new insights into the pathophysiology of LHON manifested by deficiency in mitochondrial tRNA^{Ala} 3' end metabolism.

Experimental procedures

Subjects and ophthalmic examinations

Three LHON Chinese Han pedigrees for this study were ascertained at the Eye Clinic of the Hebei Provincial Eye Hospital (Fig. S1) (39). This study was in compliance with the Declaration of Helsinki. Informed consent, blood samples, and clinical evaluations were obtained from all participating family members under protocols approved by the Ethic Committees of Zhejiang University. A comprehensive history and physical examination for these participating subjects were performed at length to identify both personal or family medical histories of visual impairment and other clinical abnormalities. The ophthalmic examinations of probands and other members of these families were

conducted as detailed previously (66–68). The degree of visual impairment was defined according to the visual acuity as follows: normal > 0.3, mild = 0.3 to 0.1; moderate < 0.1 to 0.05; severe < 0.05 to 0.02; and profound < 0.02 (6). A total of 485 control DNA samples were obtained from adult Han Chinese from the same area.

Cell lines and culture conditions

Immortalized lymphoblastoid cell lines were generated from one affected subject (III2) of the Chinese family (HZL003) carrying the m.5587A>G mutation and one genetically unrelated Chinese control individual (C15) belonging to the same mtDNA haplogroup F1 but lacking the mutation (Supplemental Methods and Table S3) (91). These cell lines were grown in RPMI 1640 medium with 10% fetal bovine serum (FBS). The bromodeoxyuridine (BrdU)-resistant 143B.TK⁻ cell line was grown in Dulbecco's Modified Eagle Medium (DMEM) (Thermo fisher) (containing 4.5 mg of glucose and 0.11 mg pyruvate/ml), supplemented with 100 µg of BrdU/ml and 5% FBS. The mtDNA-less ρ^o206 cell line, derived from 143B.TK⁻ cells, was grown under the same conditions as the parental line, except for the addition of 50 µg of uridine/ml. Transformation by cytoplasts of mtDNA-less ρ^o206 cells using one affected subject (III2) carrying the m.5587A>G mutation and one control individual was performed as described elsewhere (43, 44). All cybrid cell lines constructed with enucleated lymphoblastoid cell lines were maintained in the same medium as the 143B.TK⁻ cell line. An analysis for the presence and level of m.5587A>G mutation was carried out as described previously (Supplemental Methods) (39). The quantification of mtDNA copy number from different cybrids was performed as detailed previously (44). Three mutant cybrids (III2-T1, III2-T6, and III2-T8) carrying the m.5587A>G mutation and three control cybrids (C15-T2, C15-T3, and C15-T5) lacking the mutation with similar mtDNA copy numbers and same karyotype were used for the biochemical characterization described below.

Mitochondrial RNase Z cleavage assay

The wild-type and mutant precursors of tRNA^{Ala} corresponding to mtDNA at positions 5655 (5') to 5567 (3') were cloned into the pCRII-TOPO vector carrying SP6 and T7 promoters (Clontech). After *Hind*III digestion, the labeled RNA substrates (89 nt for tRNA^{Ala}) were transcribed with T7 RNA polymerase in the presence of 10 µM ATP, CTP, GTP, and UTP, pH 7.5, and 10 units RNase inhibitor at 20 °C. Transcripts were purified by denaturing 10% polyacrylamide gel electrophoresis (PAGE) [8 M urea, 8% polyacrylamide/bisacrylamide (19:1)] and were dissolved in 1 mM EDTA. Mitochondrial RNase Z was reconstituted from purified recombinant proteins ELAC2 as detailed elsewhere (16). The reaction mixtures were incubated in 20 µl assay buffer containing 20 mM HEPES (pH 7.6), 20 mM KCl, 2 mM MgCl₂, 2 mM DTT, 0.1 mg/ml bovine serum albumin (BSA), 80 µM S-adenosyl-methionine (SAM), 1 U RiboLock RNase Inhibitor (Thermo Fisher Scientific),

300 ng pre-tRNAs, 800 nM ELAC2. After 5, 10, 15, 20, 25, and 40 min, aliquots were withdrawn and stopped by addition of loading buffer (85% formamide, 10 mM EDTA). The reaction products were separated by denaturing 10% PAGE in 1 × Tris-borate-EDTA (TBE) buffer. After electrophoresis, the reaction products were visualized by staining with NA-Red (Beyotime).

Mitochondrial tRNA CCA-adding activity assays

The CCA tRNA nucleotidyltransferase assays were carried out in assay buffer containing 20 mM K-HEPES pH 7.6, 30 mM KCl, 5 mM MgCl₂, 0.5 mM NTPs, 2 mM DTT, and 0.1 mg/ml BSA using 200 nM pre-tRNA^{Ala} samples and 50 nM CCA-adding enzyme. The reaction mixes were preincubated at 30 °C for 10 min, and the reaction was initiated by the addition of CCA-adding enzyme TRNT1 (30). After 5, 10, 15, 20, 25, and 40 min at 30 °C, aliquots were withdrawn and stopped by addition of loading buffer (85% formamide, 10 mM EDTA). The reaction products were separated by denaturing 10% PAGE in 1 × TBE buffer and visualized by staining with NA-Red (Beyotime) (16).

UV melting assays

UV melting assays were carried out, as described previously (47, 92). The wild-type and mutant tRNA^{Ala} transcripts were generated as described above. The tRNA^{Ala} transcripts were diluted in a buffer including 50 mM sodium phosphate (pH 7.0), 50 mM NaCl, 5 mM MgCl₂, and 0.1 mM EDTA. Absorbance against temperature melting curves was measured at 260 nm with a heating rate of 1 °C/min from 25 to 95 °C through Agilent Cary 100 UV Spectrophotometer.

Mitochondrial tRNA analysis

RNAs were obtained by using TOTALLY RNA kit (Ambion) from intact cells or mitochondria isolated from mutant and control cell lines (~2 × 10⁸ cells), as detailed elsewhere (93). For tRNA Northern blot analysis, 10 µg of RNAs was electrophoresed through a 10% polyacrylamide/8 M urea gel in TBE (after heating the sample at 65 °C for 10 min). The gels were then electroblotted onto a positively charged nylon membrane (Roche) for the hybridization analysis with DIG-labeled oligodeoxynucleotide probes for 22 mitochondrial tRNAs and 5S rRNA as detailed previously (7, 31, 47). DIG-labeled oligodeoxynucleotides were generated by using DIG oligonucleotide Tailing kit (Roche). The hybridization and quantification of density in each band were performed as detailed elsewhere (7, 31, 47, 58).

For the aminoacylation assays, total cellular RNAs were isolated under acid conditions, and 10 µg of total cellular RNAs was electrophoresed at 4 °C through an acid (pH 5.0) 10% polyacrylamide/8 M urea gel to separate the charged and uncharged tRNA as detailed elsewhere (47, 48). To further distinguish nonaminoacylated tRNA from aminoacylated tRNA, samples of tRNAs were deacylated by being heated for 10 min at 60 °C (pH 8.3) and then run in parallel (47, 48). The gels were then electroblotted onto a positively charged nylon membrane (Roche) for the hybridization

analysis with oligodeoxynucleotide probes as described above. Quantification of density in each band was performed as detailed previously (47, 48).

For the tRNA mobility shift assay, 10 µg of total cellular RNAs was electrophoresed through a 10% polyacrylamide native gel at 4 °C with 50 mM Tris-glycine buffer. After electrophoresis, the gels were treated according to the Northern blot analysis as described above (47).

Western blot analysis

Western blotting analysis was performed as detailed elsewhere (53). Five micrograms of total proteins obtained from lysed mitochondria was denatured and loaded on sodium dodecyl sulfate (SDS) polyacrylamide gels. The gels were electroblotted onto a polyvinylidene difluoride (PVDF) membrane for hybridization. The antibodies used for this investigation were from Abcam [ND5 (ab92624), CO2 (ab110258), catalase (ab52477), cytochrome c (ab133504), P62 (ab56416), p62 (ab56416)], Sigma [ND6 (SAB2108622)], Proteintech Group [ND1 (19703-1-AP), SOD1 (10269-1-AP), SOD2 (24127-1-AP), GAPDH (60004-1-Ig), CYTB (55090-1-AP) and ATP8 (26723-1-AP)], ABclonal Technology [ND3(A9940), CO1 (A17889), CO3 (A9939) and ATP6 (A8193)], Cell Signaling Technology [PARP (9542), caspase 3 (14420), caspase 9 (9508), and LC3I/II (12741)], Novus [ND4 (NBP2-47365)]. Peroxidase AffiniPure goat anti-mouse IgG and goat anti-rabbit IgG (Beyotime) were used as a secondary antibody and protein signals were detected using the ECL system (Millipore). Quantification of density in each band was performed as detailed previously (53, 56).

Blue native electrophoresis analysis

BN-PAGE was performed by isolating mitochondrial proteins from mutant and control cell lines, as detailed elsewhere (51, 94). Samples containing 30 µg of total cellular proteins were separated on 3 to 12% Bis-Tris Native PAGE gel. The native gels were prewashed in cold water and then incubated with the substrates of complex I, complex II, and complex IV at room temperature as described elsewhere (52, 59). After stopping reaction with 10% acetic acid, gels were washed with water and scanned to visualize the activities of respiratory chain complexes.

Assays of activities of respiratory chain complexes

The enzymatic activities of complexes I, II, III, and IV were assayed as detailed elsewhere (95, 96).

Measurements of oxygen consumption

The OCR in various cybrid cell lines were measured with a Seahorse Bioscience XF-96 extracellular flux analyzer (Seahorse Bioscience), as detailed previously (50, 53). Cells were seeded at a density of 2 × 10⁴ cells per well on Seahorse XF96 polystyrene tissue culture plates (Seahorse Bioscience). Inhibitors were used at the following concentrations: oligomycin (1.5 µM), FCCP (0.8 µM), antimycin A (1.5 µM), and rotenone (3 µM), respectively.

Mechanism for mitochondrial tRNA 3'-end deficiency

ATP measurements

The Cell Titer-Glo Luminescent Cell Viability Assay kit (Promega) was used for the measurement of cellular and mitochondrial ATP levels, according to the modified manufacturer's instructions, as described previously (53).

Assessment of mitochondrial membrane potential

Mitochondrial membrane potential was assessed with JC-10 Assay Kit-Microplate (Abcam) following general manufacturer's recommendations with some modifications, as detailed elsewhere (54).

Measurement of ROS production

ROS measurements were performed following the procedures, as detailed previously (30, 55).

Immunofluorescence analysis

Immunofluorescence experiments were undertaken as described elsewhere (59). Cells were cultured on cover glass slips (Thermo Fisher), fixed in 4% formaldehyde for 15 min, permeabilized with 0.2% Triton X-100, blocked with 5% FBS for 1 h, and immunostained with TOM20, cytochrome C, and LAMP1 antibodies overnight at 4 °C, respectively. The cells were then incubated with Alex Fluor 594 goat anti-rabbit IgG (H+L) and Alex Fluor 488 goat anti-mouse IgG (H+L) (Thermo Fisher), stained with 4', 6-diamidino-2-phenylindole (DAPI; Invitrogen) for 15 min and mounted with Fluoromount (Sigma-Aldrich). Cells were examined using a confocal fluorescence microscope (Olympus Fluoview FV1000) with three lasers (Ex/Em = 550/570, 492/520, and 358/461 nm).

Statistical analysis

Statistical analysis was carried out using the unpaired, two-tailed Student's *t*-test contained in the Microsoft-Excel program or Macintosh (version 2019). Differences were considered significant at a $p < 0.05$.

Data availability

Representative experiments are shown in the Figures and supplemental materials. For any additional information, please contact the corresponding author.

Supporting information—This article contains [supporting information](#).

Acknowledgments—This work was supported by grants from the National Natural Science Foundation of China (31970557, 82071007); the National Key research and Development Program (2018YFC1004802), Zhejiang Provincial Public Welfare Technology Applied Research Projects (LGF21C060001) and Zhejiang Provincial Traditional Chinese Medicine Research Projects (2019ZB072), Zhejiang Provincial Natural Science Foundation of China (LY19H130005 and LY20C060003), Zhejiang Provincial Health Technology Project Commission (2019RC200), and Wenzhou

Science and Technology Bureau (Y20190067). We thank Ms Jiji Sun's technical assistance.

Author contributions—Y. J., Z. N., F. M., C. H., H. C., L. J., M. C., M. Z., J. Z., M. L., and M.-X. G. data curation; Y. J. and M.-X. G. formal analysis; Y. J., Z. N., J. Z., and M. W. validation; Y. J., Z. N., F. M., and L. J. investigation; Y. J. visualization; Y. J., Z. N., F. M., and C. H., methodology; Y. J. and M.-X. G. writing—original draft; M. Z., J. Z., and M.-X. G. resources; M. W. and M.-X. G. project administration; M.-X. G. conceptualization; M.-X. G. supervision; M.-X. G. funding acquisition; M.-X. G. Writing-review and editing.

Conflict of interest—All authors declare that they have no conflict of interest with contents of this article.

Abbreviations—The abbreviations used are: A73, adenosine at position 73; LAMP1, lysosome-associated membrane glycoprotein 1; LHON, Leber's hereditary optic neuropathy; mtDNA, mitochondrial DNA; OCR, oxygen consumption rate; OXPHOS, oxidative phosphorylation system; PARP, poly ADP ribose polymerase; RGC, retinal ganglion cell; ROS, reactive oxidative species; TBE, Tris-borate-EDTA; TRNT1, tRNA nucleotidyltransferase.

References

1. Phizicky, E. M., and Hopper, A. K. (2010) tRNA biology charges to the front. *Genes Dev.* **24**, 1832–1860
2. Pearce, S. F., Rebelo-Guiomar, P., D'Souza, A. R., Powell, C. A., Van Haute, L., and Minczuk, M. (2017) Regulation of mammalian mitochondrial gene expression: Recent advances. *Trends Biochem. Sci.* **42**, 625–639
3. Suzuki, T., Nagao, A., and Suzuki, T. (2011) Human mitochondrial tRNAs: Biogenesis, function, structural aspects, and diseases. *Annu. Rev. Genet.* **45**, 299–329
4. Van Haute, L., Pearce, S. F., Powell, C. A., D'Souza, A. R., Nicholls, T. J., and Minczuk, M. (2015) Mitochondrial transcript maturation and its disorders. *J. Inherit. Metab. Dis.* **38**, 655–680
5. Bohnsack, M. T., and Sloan, K. E. (2018) The mitochondrial epitranscriptome: The roles of RNA modifications in mitochondrial translation and human disease. *Cell. Mol. Life Sci.* **75**, 241–260
6. Qu, J., Li, R., Tong, Y., Lu, F., Qian, Y., Hu, Y., Mo, J. Q., West, C. E., and Guan, M. X. (2006) The novel A4435G mutation in the mitochondrial tRNA^{Met} may modulate the phenotypic expression of the LHON-associated ND4 G11778A mutation. *Invest. Ophthalmol. Vis. Sci.* **7**, 475–483
7. Xiao, Y., Wang, M., He, Q., Xu, L., Zhang, Q., Meng, F., Jia, Z., Zhang, F., Wang, H., and Guan, M. X. (2020) Asymmetrical effects of deafness-associated mitochondrial DNA 7516delA mutation on the processing of RNAs in the H-strand and L-strand polycistronic transcripts. *Nucleic Acids Res.* **48**, 11113–11129
8. Wang, S., Li, R., Fettermann, A., Li, Z., Qian, Y., Liu, Y., Wang, X., Zhou, A., Mo, J. Q., Yang, L., Jiang, P., Taschner, A., Rossmannith, W., and Guan, M. X. (2011) Maternally inherited essential hypertension is associated with the novel 4263A>G mutation in the mitochondrial tRNA^{Leu} gene in a large Han Chinese family. *Circ. Res.* **108**, 862–870
9. Sanchez, M. I., Mercer, T. R., Davies, S. M., Shearwood, A. M., Nygard, K. K., Richman, T. R., Mattick, J. S., Rackham, O., and Filipovska, A. (2011) RNA processing in human mitochondria. *Cell Cycle* **10**, 2904–2916
10. Scarpulla, R. C. (2008) Transcriptional paradigms in mammalian mitochondrial biogenesis and function. *Physiol. Rev.* **88**, 611–638
11. Anderson, S., Bankier, A. T., Barrell, B. G., de Bruijn, M. H., Coulson, A. R., Drouin, J., Eperon, I. C., Nierlich, D. P., Roe, B. A., Sanger, F., Schreier, P. H., Smith, A. J., Staden, R., and Young, I. G. (1981) Sequence and organization of the human mitochondrial genome. *Nature* **290**, 457–465

12. Montoya, J., Gaines, G. L., and Attardi, G. (1983) The pattern of transcription of the human mitochondrial rRNA genes reveals two overlapping transcription units. *Cell* **34**, 151–159
13. Mercer, T. R., Neph, S., Dinger, M. E., Crawford, J., Smith, M. A., Shearwood, A. M., Haugen, E., Bracken, C. P., Rackham, O., Stamatoyannopoulos, J. A., Filipovska, A., and Mattick, J. S. (2011) The human mitochondrial transcriptome. *Cell* **146**, 645–658
14. Ojala, D., Montoya, J., and Attardi, G. (1981) tRNA punctuation model of RNA processing in human mitochondria. *Nature* **290**, 470–474
15. Brzezniak, L. K., Bijata, M., Szczesny, R. J., and Stepien, P. P. (2011) Involvement of human ELAC2 gene product in 3' end processing of mitochondrial tRNAs. *RNA Biol.* **8**, 616–626
16. Reinhard, L., Sridhara, S., and Hallberg, B. M. (2017) The MRPP1/MRPP2 complex is a tRNA-maturation platform in human mitochondria. *Nucleic Acids Res.* **45**, 12469–12480
17. Nagaike, T., Suzuki, T., Tomari, Y., Takemoto-Hori, C., Negayama, F., Watanabe, K., and Ueda, T. (2001) Identification and characterization of mammalian mitochondrial tRNA nucleotidyltransferases. *J. Biol. Chem.* **276**, 40041–40049
18. Shi, P. Y., Maizels, N., and Weiner, A. M. (1998) CCA addition by tRNA nucleotidyltransferase: Polymerization without translocation? *EMBO J.* **17**, 3197–3206
19. Hou, Y. M. (2010) CCA addition to tRNA: Implications for tRNA quality control. *IUBMB Life* **62**, 251–260
20. Suzuki, T., Yashiro, Y., Kikuchi, I., Ishigami, Y., Saito, H., Matsuzawa, I., Okada, S., Mito, M., Iwasaki, S., Ma, D., Zhao, X., Asano, K., Lin, H., Kirino, Y., Sakaguchi, Y., et al. (2020) Complete chemical structures of human mitochondrial tRNAs. *Nat. Commun.* **11**, 4269
21. Guan, M. X., Yan, Q., Li, X., Bykhovskaya, Y., Gallo-Teran, J., Hajek, P., Umeda, N., Zhao, H., Garrido, G., Mengesha, E., Suzuki, T., del Castillo, I., Peters, J. L., Li, R., Qian, Y., et al. (2006) Mutation in TRMU related to transfer RNA modification modulates the phenotypic expression of the deafness-associated mitochondrial 12S ribosomal RNA mutations. *Am. J. Hum. Genet.* **79**, 291–302
22. Meng, F., Zhou, M., Xiao, Y., Mao, X., Zheng, J., Lin, J., Lin, T., Ye, Z., Cang, X., Fu, Y., Wang, M., and Guan, M. X. (2021) A deafness-associated tRNA mutation caused pleiotropic effects on the m¹G37 modification, processing, stability and aminoacylation of tRNA^{Ile} and mitochondrial translation. *Nucleic Acids Res.* **49**, 1075–1093
23. Peng, G. X., Zhang, Y., Wang, Q. Q., Li, Q. R., Xu, H., Wang, E. D., and Zhou, X. L. (2021) The human tRNA taurine modification enzyme GTPBP3 is an active GTPase linked to mitochondrial diseases. *Nucleic Acids Res.* **49**, 2816–2834
24. Zhang, Q., He, X., Yao, S., Lin, T., Zhang, L., Chen, D., Chen, C., Yang, Q., Li, F., Zhu, Y. M., and Guan, M. X. (2021) Ablation of Mto1 in zebrafish exhibited hypertrophic cardiomyopathy manifested by mitochondrion RNA maturation deficiency. *Nucleic Acids Res.* **49**, 4689–4704
25. Sissler, M., González-Serrano, L. E., and Westhof, E. (2017) Recent advances in mitochondrial aminoacyl-tRNA synthetases and disease. *Trends Mol. Med.* **23**, 693–708
26. Ibba, M., and Soll, D. (2000) Aminoacyl-tRNA synthesis. *Annu. Rev. Biochem.* **69**, 617–650
27. Zeng, Q. Y., Peng, G. X., Li, G., Zhou, J. B., Zheng, W. Q., Xue, M. Q., Wang, E. D., and Zhou, X. L. (2019) The G3-U70-independent tRNA recognition by human mitochondrial alanyl-tRNA synthetase. *Nucleic Acids Res.* **47**, 3072–3085
28. Levinger, L., Mörl, M., and Florentz, C. (2004) Mitochondrial tRNA 3' end metabolism and human disease. *Nucleic Acids Res.* **32**, 5430–5441
29. Xue, L., Wang, M., Li, H., Wang, H., Jiang, F., Hou, L., Geng, J., Lin, Z., Peng, Y., Zhou, H., Yu, H., Jiang, P., Mo, J. Q., and Guan, M. X. (2016) Mitochondrial tRNA mutations in 2070 Chinese Han subjects with hypertension. *Mitochondrion* **30**, 208–221
30. Jiang, P., Wang, M., Xue, L., Xiao, Y., Yu, J., Wang, H., Yao, J., Liu, H., Peng, Y., Liu, H., Li, H., Chen, Y., and Guan, M. X. (2016) A hypertension-associated tRNA^{Ala} mutation alters tRNA metabolism and mitochondrial function. *Mol. Cell Biol.* **36**, 1920–1930
31. Zhao, X., Cui, L., Xiao, Y., Mao, Q., Aishanjiang, M., Kong, W., Liu, Y., Chen, H., Hong, F., Jia, Z., Wang, M., Jiang, P., and Guan, M. X. (2019) Hypertension-associated mitochondrial DNA 4401A>G mutation caused the aberrant processing of tRNA^{Met}, all 8 tRNAs and ND6 mRNA in the light-strand transcript. *Nucleic Acids Res.* **47**, 10340–10356
32. Yan, H., Zareen, N., and Levinger, L. (2006) Naturally occurring mutations in human mitochondrial pre-tRNA^{Ser(UCN)} can affect the transfer ribonuclease Z cleavage site, processing kinetics, and substrate secondary structure. *J. Biol. Chem.* **281**, 3926–3935
33. Levinger, L., Giegé, R., and Florentz, C. (2003) Pathology-related substitutions in human mitochondrial tRNA^{Ile} reduce precursor 3' end processing efficiency *in vitro*. *Nucleic Acids Res.* **31**, 1904–1912
34. Levinger, L., and Serjanov, D. (2012) Pathogenesis-related mutations in the T-loops of human mitochondrial tRNAs affect 3' end processing and tRNA structure. *RNA Biol.* **9**, 283–291
35. Guan, M. X., Enriquez, J. A., Fischel-Ghodsian, N., Puranam, R. S., Lin, C. P., Maw, M. A., and Attardi, G. (1998) The deafness-associated mitochondrial DNA mutation at position 7445, which affects tRNA^{Ser(UCN)} precursor processing, has long-range effects on NADH dehydrogenase subunit ND6 gene expression. *Mol. Cell Biol.* **18**, 5868–5879
36. Slade, A., Kattini, R., Campbell, C., and Holcik, M. (2020) Diseases associated with defects in tRNA CCA addition. *Int. J. Mol. Sci.* **21**, 3780
37. Wedatilake, Y., Niazi, R., Fassone, E., Powell, C. A., Pearce, S., Plagnol, V., Saldanha, J. W., Kleta, R., Chong, W. K., Footitt, E., Mills, P. B., Taanman, J. W., Minczuk, M., Clayton, P. T., and Rahman, S. (2016) TRNT1 deficiency: Clinical, biochemical and molecular genetic features. *Orphanet J. Rare Dis.* **11**, 90
38. Sasarman, F., Thiffault, I., Weraarpachai, W., Salomon, S., Maftai, C., Gauthier, J., Ellazam, B., Webb, N., Antonicka, H., Janer, A., Brunel-Guitton, C., Elpeleg, O., Mitchell, G., and Shoubridge, E. A. (2015) The 3' addition of CCA to mitochondrial tRNA^{Ser(AGY)} is specifically impaired in patients with mutations in the tRNA nucleotidyl transferase TRNT1. *Hum. Mol. Genet.* **24**, 2841–2847
39. Ji, Y., Qiao, L., Liang, X., Zhu, L., Gao, Y., Zhang, J., Jia, Z., Wei, Q. P., Liu, X., Jiang, P., and Guan, M. X. (2017) Leber's hereditary optic neuropathy is potentially associated with a novel m.5587T>C mutation in two pedigrees. *Mol. Med. Rep.* **16**, 8997–9004
40. Kuhle, B., Chihade, J., and Schimmel, P. (2020) Relaxed sequence constraints favor mutational freedom in idiosyncratic metazoan mitochondrial tRNAs. *Nat. Commun.* **11**, 969
41. Salinas-Giegé, T., Giegé, R., and Giegé, P. (2015) tRNA biology in mitochondria. *Int. J. Mol. Sci.* **16**, 4518–4559
42. Wende, S., Bonin, S., Götze, O., Betat, H., and Mörl, M. (2015) The identity of the discriminator base has an impact on CCA addition. *Nucleic Acids Res.* **43**, 5617–5629
43. King, M. P., and Attardi, G. (1996) Mitochondria-mediated transformation of human ρ^0 cells. *Methods Enzymol.* **264**, 313–334
44. Zhang, J., Ji, Y., Lu, Y., Fu, R., Xu, M., Liu, X., and Guan, M. X. (2018) Leber's hereditary optic neuropathy (LHON)-associated ND5 12338T>C mutation altered the assembly and function of complex I, apoptosis and autophagy. *Hum. Mol. Genet.* **27**, 1999–2011
45. Gamper, H., and Hou, Y. M. (2018) tRNA 3'-amino-tailing for stable amino acid attachment. *RNA* **24**, 1878–1885
46. Wang, M., Zhou, X. L., Liu, R. J., Fang, Z. P., Zhou, M., Erian, i G., and Wang, E. D. (2013) Multilevel functional and structural defects induced by two pathogenic mitochondrial tRNA mutations. *Biochem. J.* **453**, 455–465
47. Zhou, M., Xue, L., Chen, Y., Li, H., He, Q., Wang, B., Meng, F., Wang, M., and Guan, M. X. (2018) A hypertension-associated mitochondrial DNA mutation introduces an m¹G37 modification into tRNA^{Met}, altering its structure and function. *J. Biol. Chem.* **293**, 1425–1438
48. Enriquez, J. A., and Attardi, G. (1996) Analysis of aminoacylation of human mitochondrial tRNAs. *Methods Enzymol.* **264**, 183–196
49. Scheffler, I. E. (2015) Mitochondrial disease associated with complex I (NADH-CoQ oxidoreductase) deficiency. *J. Inher. Metab. Dis.* **38**, 405–415
50. Dranka, B. P., Benavides, G. A., Diers, A. R., Giordano, S., Zelickson, B. R., Reily, C., Zou, L., Chatham, J. C., Hill, B. G., Zhang, J., Landar, A., and Darley-Usmar, V. M. (2011) Assessing bioenergetic function in response to oxidative stress by metabolic profiling. *Free Radic. Biol. Med.* **51**, 1621–1635

Mechanism for mitochondrial tRNA 3'-end deficiency

51. Jha, P., Wang, X., and Auwerx, J. (2016) Analysis of mitochondrial respiratory chain super-complexes using blue native polyacrylamide gel electrophoresis (BN-PAGE). *Curr. Protoc. Mouse Biol.* **6**, 1–14
52. Jin, X., Zhang, Z., Nie, Z., Wang, C., Meng, F., Yi, Q., Chen, M., Sun, J., Zou, J., Jiang, P., and Guan, M. X. (2021) An animal model for mitochondrial tyrosyl-tRNA synthetase deficiency reveals links between oxidative phosphorylation and retinal function. *J. Biol. Chem.* **296**, 100437
53. Gong, S., Peng, Y., Jiang, P., Wang, M., Fan, M., Wang, X., Zhou, H., Li, H., Yan, Q., Huang, T., and Guan, M. X. (2014) A deafness-associated tRNA^{His} mutation alters the mitochondrial function, ROS production and membrane potential. *Nucleic Acids Res.* **42**, 8039–8048
54. Reers, M., Smiley, S. T., Mottola-Hartshorn, C., Chen, A., Lin, M., and Chen, L. B. (1995) Mitochondrial membrane potential monitored by JC-1 dye. *Methods Enzymol.* **260**, 406–417
55. Mahfouz, R., Sharma, R., Lackner, J., Aziz, N., and Agarwal, A. (2009) Evaluation of chemiluminescence and flow cytometry as tools in assessing production of hydrogen peroxide and superoxide anion in human spermatozoa. *Fertil. Steril.* **92**, 819–827
56. Gong, S., Wang, X., Meng, F., Cui, L., Yi, Q., Zhao, Q., Cang, X., Cai, Z., Mo, J. Q., Liang, Y., and Guan, M. X. (2020) Overexpression of mitochondrial histidyl-tRNA synthetase restores mitochondrial dysfunction caused by a deafness-associated tRNA^{His} mutation. *J. Biol. Chem.* **295**, 940–954
57. Schieber, M., and Chandel, N. S. (2014) ROS function in redox signaling and oxidative stress. *Curr. Biol.* **24**, R453–R462
58. Jia, Z., Zhang, Y., Li, Q., Ye, Z., Liu, Y., Fu, C., Cang, X., Wang, M., and Guan, M. X. (2019) A coronary artery disease-associated tRNA^{Thr} mutation altered mitochondrial function, apoptosis and angiogenesis. *Nucleic Acids Res.* **47**, 2056–2074
59. Ji, Y., Zhang, J., Lu, Y., Yi, Q., Chen, M., Xie, S., Mao, X., Xiao, Y., Meng, F., Zhang, M., Yang, R., and Guan, M. X. (2020) Complex I mutations synergize to worsen the phenotypic expression of Leber's hereditary optic neuropathy. *J. Biol. Chem.* **295**, 13224–13238
60. Taylor, R. C., Cullen, S. P., and Martin, S. J. (2008) Apoptosis: Controlled demolition at the cellular level. *Nat. Rev. Mol. Cell Biol.* **9**, 231–241
61. Anding, A. L., and Baehrecke, E. H. (2017) Cleaning house: Selective autophagy of organelles. *Dev. Cell* **41**, 10–22
62. Korolchuk, V. I., Menzies, F. M., and Rubinsztein, D. C. (2009) A novel link between autophagy and the ubiquitin-proteasome system. *Autophagy* **5**, 862–863
63. Zhu, Y., Chen, G., Chen, L., Zhang, W., Feng, D., Liu, L., and Chen, Q. (2014) Monitoring autophagy in mammalian cells. *Methods Enzymol.* **547**, 39–55
64. Wallace, D. C., and Lott, M. T. (2017) Leber hereditary optic neuropathy: Exemplar of an mtDNA disease. *Handb. Exp. Pharmacol.* **240**, 339–376
65. Wallace, D. C., Singh, G., Lott, M. T., Hodge, J. A., Schurr, T. G., Lezza, A. M., Elsas, L. J., and Nikoskelainen, E. K. (1998) Mitochondrial DNA mutation associated with Leber's hereditary optic neuropathy. *Science* **242**, 1427–1430
66. Jiang, P., Liang, M., Zhang, J., Gao, Y., He, Z., Yu, H., Zhao, F., Ji, Y., Liu, X., Zhang, M., Fu, Q., Tong, Y., Sun, Y., Zhou, X., Huang, T., et al. (2015) Prevalence of mitochondrial ND4 mutations in 1281 Han Chinese subjects with Leber's hereditary optic neuropathy. *Invest. Ophthalmol. Vis. Sci.* **56**, 4778–4788
67. Ji, Y., Liang, M., Zhang, J., Zhu, L., Zhang, Z., Fu, R., Liu, X., Zhang, M., Fu, Q., Zhao, F., Tong, Y., Sun, Y., Jiang, O., and Guan, M. X. (2016) Mitochondrial ND1 variants in 1281 Chinese subjects with Leber's hereditary optic neuropathy. *Invest. Ophthalmol. Vis. Sci.* **57**, 2377–2389
68. Liang, M., Jiang, P., Li, F., Zhang, J., Ji, Y., He, Y., Xu, M., Zhu, J., Meng, X., Zhao, F., Tong, Y., Liu, X., Sun, Y., Zhou, X., Mo, J. Q., et al. (2014) Frequency and spectrum of mitochondrial ND6 mutations in 1218 Han Chinese subjects with Leber's hereditary optic neuropathy. *Invest. Ophthalmol. Vis. Sci.* **55**, 1321–1331
69. Miao, Z., and Westhof, E. (2017) RNA structure: Advances and assessment of 3D structure prediction. *Annu. Rev. Biophys.* **46**, 483–503
70. Lovato, M. A., Chihade, J. W., and Schimmel, P. (2001) Translocation within the acceptor helix of a major tRNA identity determinant. *EMBO J.* **20**, 846–8453
71. Giege, R., Sissler, M., and Florentz, C. (1998) Universal rules and idiosyncratic features in tRNA identity. *Nucleic Acids Res.* **26**, 5017–5035
72. Nagan, M. C., Beuning, P., Musier-Forsyth, K., and Cramer, C. J. (2000) Importance of discriminator base stacking interactions: Molecular dynamics analysis of A73 microhelix^{Ala} variants. *Nucleic Acids Res.* **28**, 2527–2534
73. Chomyn, A., Enriquez, J. A., Micol, V., Fernandez-Silva, P., and Attardi, G. (2000) The mitochondrial myopathy, encephalopathy, lactic acidosis, and stroke-like episode syndrome-associated human mitochondrial tRNA^{Leu(UUR)} mutation causes aminoacylation deficiency and concomitant reduced association of mRNA with ribosomes. *J. Biol. Chem.* **275**, 19198–19209
74. Wang, M., Peng, Y., Zheng, J., Zheng, B., Jin, X., Liu, H., Wang, Y., Tang, X., Huang, T., Jiang, P., and Guan, M. X. (2016) A deafness-associated tRNA^{Asp} mutation alters the m¹G37 modification, aminoacylation and stability of tRNA^{Asp} and mitochondrial function. *Nucleic Acids Res.* **44**, 10974–10985
75. Wallace, D. C. (2005) A mitochondrial paradigm of metabolic and degenerative diseases, aging, and cancer: A dawn for evolutionary medicine. *Annu. Rev. Genet.* **39**, 359–407
76. Raimundo, N., Song, L., Shutt, T. E., McKay, S. E., Cotney, J., Guan, M. X., Gilliland, T. C., Hohuan, D., Santos-Sacchi, J., and Shadel, G. S. (2012) Mitochondrial stress engages E2F1 apoptotic signaling to cause deafness. *Cell* **148**, 716–726
77. Country, M. W. (2017) Retinal metabolism: A comparative look at energetics in the retina. *Brain Res.* **1672**, 50–57
78. Wong-Riley, M. T. (2010) Energy metabolism of the visual system. *Eye Brain* **2**, 99–116
79. Wong, A., Cavelier, L., Collins-Schramm, H. E., Seldin, M. F., McGrogan, M., Savontaus, M. L., and Cortopassi, G. A. (2002) Differentiation-specific effects of LHON mutations introduced into neuronal NT2 cells. *Hum. Mol. Genet.* **11**, 431–438
80. Song, L., Yu, A., Murray, K., and Cortopassi, G. (2017) Bipolar cell reduction precedes retinal ganglion neuron loss in a complex I knockout mouse model. *Brain Res.* **165**, 232–244
81. Melser, S., Lavie, J., and Bénard, G. (2015) Mitochondrial degradation and energy metabolism. *Biochim. Biophys. Acta* **1853**, 2812–2821
82. Lee, J., Giodano, S., and Zhang, J. (2012) Autophagy, mitochondria and oxidative stress: Cross-talk and redox signaling. *Biochem. J.* **44**, 523–540
83. Youle, R. J., and Narendra, D. P. (2011) Mechanisms of autophagy. *Nat. Rev. Mol. Cell Biol.* **12**, 9–14
84. Yu, J., Liang, X., Ji, Y., Ai, C., Liu, J., Zhu, L., Nie, Z., Jin, X., Wang, C., Zhang, J., Zhao, F., Mei, S., Zhao, X., Zhou, X., Zhang, M., et al. (2020) PRICKLE3 linked to ATPase biogenesis manifested Leber's Hereditary Optic Neuropathy. *J. Clin. Invest.* **130**, 4935–4946
85. Jiang, P., Jin, X., Peng, Y., Wang, M., Liu, H., Liu, X., Zhang, Z., Ji, Y., Zhang, J., Liang, M., Zhao, F., Sun, Y. H., Zhang, M., Zhou, X., Chen, Y., et al. (2016) The exome sequencing identified the mutation in YARS2 encoding the mitochondrial tyrosyl-tRNA synthetase as a nuclear modifier for the phenotypic manifestation of Leber's hereditary optic neuropathy-associated mitochondrial DNA mutation. *Hum. Mol. Genet.* **25**, 584–596
86. Torres, A. G., Reina, O., Stephan-Otto Attolini, C., and Ribas de Pouplana, L. (2019) Differential expression of human tRNA genes drives the abundance of tRNA-derived fragments. *Proc. Natl. Acad. Sci. U. S. A.* **116**, 8451–8456
87. Dittmar, K. A., Goodenbour, J. M., and Pan, T. (2006) Tissue-specific differences in human transfer RNA expression. *PLoS Genet.* **2**, e221
88. Ma, Y. Y., Wu, T. F., Liu, Y. P., Wang, Q., Song, J. Q., Li, X. Y., Shi, X. Y., Zhang, W. N., Zhao, M., Hu, L. Y., Yang, Y. L., and Zou, L. P. (2013) Genetic and biochemical findings in Chinese children with Leigh syndrome. *J. Clin. Neurosci.* **20**, 1591–1594
89. Agnew, T., Goldsworthy, M., Aguilar, C., Morgan, A., Simon, M., Hilton, H., Esapa, C., Wu, Y., Cater, H., Bentley, L., Scudamore, C., Poulton, J., Morten, K. J., Thompson, K., He, L., et al. (2018) A Wars2 mutant mouse model displays OXPHOS deficiencies and activation of tissue-specific stress response pathways. *Cell Rep.* **25**, 3315–3328
90. Dogan, S. A., Pujol, C., Maiti, P., Kukat, A., Wang, S., Hermans, S., Senft, K., Wibom, R., Rugarli, E. L., and Trifunovic, A. (2014) Tissue-specific loss of DARS2 activates stress responses independently of respiratory chain deficiency in the heart. *Cell Metab.* **19**, 458–469

91. Miller, G., and Lipman, M. (1973) Release of infectious Epstein–Barr virus by transformed marmoset leukocytes. *Proc. Natl. Acad. Sci. U. S. A.* **70**, 190–194
92. Wang, M., Liu, H., Zheng, J., Chen, B., Zhou, M., Fan, W., Wang, H., Liang, X., Zhou, X., Eriani, G., Jiang, P., and Guan, M. X. (2016) A deafness- and diabetes-associated trna mutation causes deficient pseudouridylation at position 55 in tRNA^{Glu} and mitochondrial dysfunction. *J. Biol. Chem.* **291**, 21029–21041
93. King, M. P., and Attardi, G. (1993) Post-transcriptional regulation of the steady-state levels of mitochondrial tRNAs in HeLa cells. *J. Biol. Chem.* **268**, 10228–10237
94. Ji, Y., Zhang, J., Yu, J., Wang, Y., Lu, Y., Liang, M., Li, Q., Jin, X., Wei, Y., Meng, F., Gao, Y., Cang, X., Tong, Y., Liu, X., Zhang, M., *et al.* (2019) Contribution of mitochondrial ND1 3394T>C mutation to the phenotypic manifestation of Leber's hereditary optic neuropathy. *Hum. Mol. Genet.* **28**, 1515–1529
95. Birch-Machin, M. A., and Turnbull, D. M. (2001) Assaying mitochondrial respiratory complex activity in mitochondria isolated from human cells and tissues. *Methods Cell Biol.* **65**, 97–117
96. Meng, F., He, Z., Tang, X., Zheng, J., Jin, X., Zhu, Y., Ren, X., Zhou, M., Wang, M., Gong, S., Mo, J. Q., Shu, Q., and Guan, M. X. (2018) Contribution of the tRNA^{Leu} 4317A>G mutation to the phenotypic manifestation of the deafness-associated mitochondrial 12S rRNA 1555A>G mutation. *J. Biol. Chem.* **293**, 3321–3334